NASA Technical Paper 2276

March 1984

Analysis of Rectangular Microstrip Antennas

M. C. Bailey and
M. D. Deshpande

NASA

NASA
Technical
Paper
2276

1984

Analysis of Rectangular Microstrip Antennas

M. C. Bailey
Langley Research Center
Hampton, Virginia

M. D. Deshpande
The George Washington University
Joint Institute for Advancement of Flight Sciences
Langley Research Center
Hampton, Virginia

National Aeronautics
and Space Administration

**Scientific and Technical
Information Branch**

INTRODUCTION

Because of many unique and attractive properties (e.g., light weight, low cost, and compatibility with integrated circuits), microstrip antennas are finding many applications. As a result, in recent years a number of theoretical and experimental methods to determine their electromagnetic properties have been proposed (ref. 1). By treating the rectangular antenna as two parallel slots interconnected by a low-impedance transmission line, it is possible to obtain some useful predictions of the radiative properties (refs. 2 and 3). However, this simple model is not adequate for predicting the variation of impedance with feed location. Furthermore, the transmission-line model cannot be applied to microstrip patch antennas other than rectangular. To analyze a wider variety of microstrip patch shapes, a cavity model has been proposed (ref. 4). Although the cavity model predicts quite accurately the radiation pattern, it requires a semiempirical correction for the resonant frequency in order to match the calculated results with the experimental data. This discrepancy may be due to the fringing field at the edges of the patch not being incorporated in the formulation and the dielectric substrate with finite thickness being replaced by a homogeneous medium of equivalent dielectric constant. There is, therefore, a need for more rigorous analysis techniques for microstrip antennas.

The rectangular and circular microstrip antennas have been analyzed by modeling the patch as a grid of wires and solving the resulting structure numerically (ref. 5). Although the method appears to be more accurate and general, it requires a lot of computer time and storage. Furthermore, to optimize the computation, it is essential to know a priori the direction of current flow on the patch.

Using the reaction integral equation in conjunction with the method of moments, Newman et al. (ref. 6) propose a method which seems to be quite accurate for predicting patch current, impedance, and resonant frequency. However, Newman's method requires an unusually precise computation of the elements in the impedance matrix while still modeling the dielectric substrate as an equivalent semi-infinite homogeneous medium.

There have been other attempts at analyzing microstrip antennas as open microstrip cavity resonators for rectangular and circular patches (refs. 7 and 8). However, these formulations do not include the patch excitation in the analytical modeling, and the techniques cannot be extended to microstrip arrays.

The purpose of the present work is to reformulate the problem to overcome the difficulties encountered in previous methods and to establish a foundation for analyzing a variety of electromagnetic problems related to printed-circuit antennas. The problem is analyzed by first deriving a dyadic Green's function which satisfies the boundary conditions for a unit current located in the plane of the microstrip patch. By weighting the Green's function with the electric current density and integrating over the patch, the radiated electromagnetic field is calculated at any point inside the dielectric. Coupled electric-field integral equations for the unknown patch current density are obtained by forcing the total tangential electric field on the patch to zero. With the proper basis and testing functions for the unknown current distribution, the integral equations are reduced to a matrix equation which may be solved for the patch current. The current distribution on the patch is then used to determine the properties of the microstrip antennas.

Some features of the present method are as follows: (1) it correctly accounts for the finite thickness of the dielectric substrate and the effect of surface waves; (2) it does not require high precision in the numerical computation of the matrix elements; (3) it allows improved convergence of the solution through proper choice of the basis and testing functions; (4) it can be extended to microstrip patches of any shape, provided one selects the proper basis functions; and (5) it is suitable for more involved problems of coupled microstrip antennas.

SYMBOLS

$\bar{A}$	magnetic vector potential
d	dielectric substrate thickness
$\bar{E}$	electric-field vector
E_o	amplitude of plane wave
E_x^i	x component of electric field due to the incident plane wave (eq. (16))
E_y^i	y component of the electric field due to the incident plane wave
$E_\theta(\theta,\phi)$	θ component of $\bar{E}$
$E_\phi(\theta,\phi)$	ϕ component of $\bar{E}$
$\bar{\bar{G}}$	dyadic Green's function
$\bar{\bar{g}}$	bidimensional Fourier transform of $\bar{\bar{G}}$
$\bar{H}$	magnetic-field vector
H_i	magnetic field due to the incident plane wave
$\bar{\bar{I}}$	unit dyadic impulse current
$\bar{J}$	surface electric current density vector
j	$\sqrt{-1}$
$\bar{j}$	bidimensional Fourier transform of $\bar{J}$
j_x	x component of $\bar{j}$
j_y	y component of $\bar{j}$
j_x	complex coefficient for x-directed current
j_y	complex coefficient for y-directed current
k	wave propagation constant in dielectric region
k_o	wave propagation constant in free space

k_x Fourier transform variable with respect to x

k_y Fourier transform variable with respect to y

k_z complex wave propagation constant in z direction

$M + 1$ number of y-directed strips (see fig. 2)

m,n m,n subdomain of field

$N + 1$ number of x-directed strips (see fig. 2)

p,q p,q subdomain of source

r,θ,ϕ coordinates of point in spherical coordinate system

W_x E-plane dimension of the rectangular patch

$(W_x/\lambda_\varepsilon)_o$ resonant width of patch

W_y H-plane dimension of the rectangular patch

x,y,z rectangular Cartesian coordinates of field point

x',y',z' rectangular Cartesian coordinates of source point

$\hat{x},\hat{y},\hat{z}$ unit vectors along x-, y-, and z-axis, respectively

Z_{xx} self-impedance of x-directed patch current (eq. (52))

$Z_{xx}^{mn,pq}$ mutual impedance between x-directed currents on m,n and p,q subdomains (eq. (37))

$Z_{xy}^{mn,pq}$ mutual impedance between x- and y-directed currents on m,n and p,q subdomains (eq. (38))

$Z_{yx}^{mn,pq}$ mutual impedance between y- and x-directed currents on m,n and p,q subdomains (eq. (39))

$Z_{yy}^{mn,pq}$ mutual impedance between y-directed currents on m,n and p,q subdomains (eq. (40))

Γ wave reflection coefficient

Δx $= W_x/M + 1$

Δy $= W_y/N + 1$

$\Delta(W_x/\lambda_\varepsilon)_3$ bandwidth for voltage standing-wave ratio (VSWR) less than 3

$\delta(x-x')$ delta function, $\frac{1}{2\pi}\int_{-\infty}^{\infty} \exp[j(x - x')w]\, dw$

ε_r relative permittivity of dielectric substrate

λ_ε wavelength in dielectric substrate

μ_ε permeability of dielectric substrate

ω angular frequency, rad/sec

Superscripts:

I dielectric region

II free space region

I/II either region I or II

THEORY

General

The geometry of the microstrip antenna is shown in figure 1. It consists of a thin conducting plate, or patch, in the form of a rectangle, a square, a circle, or other geometric shapes embedded in a dielectric substrate, with one surface being grounded by a perfectly conducting plane. Usually the microstrip antenna is excited either by a microstrip transmission line connected to one edge of the patch or by a coaxial probe with the center conductor extending through the ground plane and connected to the patch. However, in order to determine the resonant frequency, the bandwidth, and the radiation pattern, it can be assumed that the patch is excited by a plane wave polarized in the x-direction and with normal incidence on the patch, as shown in figure 1. This model gives results which are valid for the practical microstrip antenna so long as the exciting mechanism does not appreciably alter the current distribution of the patch. For the dielectric substrate with a thickness less than $0.1\lambda_\varepsilon$, which is the case for most of the practical microstrip antennas, the dimensions of the exciting mechanism are much less than $1.0\lambda_\varepsilon$ and, therefore, the feed connection produces only a small perturbation in the radiation characteristics of the antenna.

The surface current induced on the patch controls the antenna properties such as radiation pattern, input impedance, resonant frequency, and bandwidth of the microstrip antenna and, therefore, must be determined first. Let $\bar{J}(x',y',z')$ be the unknown surface electric current density present on the patch. For a very thin patch in the plane $z = z'$, $\bar{J}$ has only x- and y-directed components. However, for the general case, it is assumed that $\bar{J}$ has all three components. The electromagnetic field due to $\bar{J}$ can be obtained from

$$\bar{H}(x,y,z) = \frac{1}{\mu} \nabla \times \bar{A}(x,y,z) \tag{1}$$

$$\bar{E}(x,y,z) = -\frac{j\omega}{k^2}\{k^2 \bar{A}(x,y,z) + \nabla[\nabla \cdot \bar{A}(x,y,z)]\} \tag{2}$$

where the assumed time variation $\exp(j\omega t)$ has been suppressed. The magnetic vector potential $\bar{A}$ must satisfy the wave equation

$$\nabla^2 \bar{A}^I(x,y,z) + k^2 \bar{A}^I(x,y,z) = -\mu \bar{J} \tag{3}$$

in the dielectric (region I) and must satisfy

$$\nabla^2 \bar{A}^{II}(x,y,z) + k_o^2 \bar{A}^{II}(x,y,z) = 0 \tag{4}$$

in free space (region II).

If $\bar{\bar{G}}^{I/II}(x,y,z,x',y',z')$ is the dyadic Green's function for regions I or II for a unit impulse current source $\bar{\bar{I}}(x',y',z')$ embedded in the dielectric substrate, then the solutions of equations (3) and (4) can be written in the form

$$\bar{A}^{I/II}(x,y,z,z') = \int\int_{\text{Patch}} \bar{J}(x',y',z') \cdot \bar{\bar{G}}^{I/II}(x,y,z,x',y',z')\, dx'\, dy' \tag{5}$$

With the dyadic Green's function from the appendix substituted into equation (5) and the order of integration changed, the magnetic vector potential due to the patch current $\bar{J}(x',y')$ can be obtained in the form

$$\bar{A}^I(x,y,z) = \frac{1}{(2\pi)^2} \int_{-\infty}^{\infty} \int_{-\infty}^{\infty} \bar{j}(k_x,k_y) \cdot \bar{\bar{f}}^I(k_x,k_y,z) \exp[j(k_x x + k_y y)]\, dk_x\, dk_y \tag{6}$$

where

$$\bar{j}(k_x,k_y) = \int\int_{\text{Patch}} \bar{J}(x',y') \exp[-j(k_x x' + k_y y')]\, dx'\, dy' \tag{7}$$

and the components of the dyadic $\bar{\bar{f}}$ are defined in the appendix.

The scattered field due to the patch current can be obtained from equation (2) in the following form:

$$E_x^I(x,y,z) = \frac{-j\omega}{(2\pi)^2 k^2} \int_{-\infty}^{\infty} \int_{-\infty}^{\infty} \left[\zeta_{xx}(k_x,k_y,z)\, j_x(k_x,k_y) + \zeta_{yx}(k_x,k_y,z)\, j_y(k_x,k_y)\right] \exp(jk_x x + jk_y y)\, dk_x\, dk_y \tag{8}$$

$$E_y^I(x,y,z) = \frac{-j\omega}{(2\pi)^2 k^2} \int_{-\infty}^{\infty} \int_{-\infty}^{\infty} \left[\zeta_{xy}(k_x,k_y,z)\, j_x(k_x,k_y) + \zeta_{yy}(k_x,k_y,z)\, j_y(k_x,k_y)\right] \exp(jk_x x + jk_y y)\, dk_x\, dk_y \tag{9}$$

$$E_z^I(x,y,z) = \frac{-j\omega}{(2\pi)^2 k^2} \int_{-\infty}^{\infty} \int_{-\infty}^{\infty} \left\{\left(k_x^2 + k_y^2\right)\left[f_{zx}^I(k_x,k_y,z) + f_{zy}^I(k_x,k_y,z)\right] + j\,\frac{\partial f_{xx}^I(k_x,k_y,z)}{\partial z}\left[k_y j_y(k_x,k_y) + k_x j_x(k_x,k_y)\right]\right\} \exp(jk_x x + jk_y y)\, dk_x\, dk_y \tag{10}$$

where

$$\zeta_{xx}(k_x,k_y,z) = \left(k^2 - k_x^2\right) f_{xx}^I + jk_x^2 \frac{\partial f_{zx}^I}{\partial z} \tag{11}$$

$$\zeta_{xy}(k_x,k_y,z) = -k_x k_y f_{xx}^I + jk_x k_y \frac{\partial f_{zx}^I}{\partial z} \tag{12}$$

$$\zeta_{yx}(k_x,k_y,z) = -k_x k_y f_{yy}^I + jk_x k_y \frac{\partial f_{zy}^I}{\partial z} \tag{13}$$

$$\zeta_{yy}(k_x,k_y,z) = (k^2 - k_y^2)f_{yy}^I + jk_y^2 \frac{\partial f_{zy}^I}{\partial z} \tag{14}$$

The total tangential electric field at the plane $z = z'$ consists of the scattered field due to the patch current and the field due to the incident plane wave. The scattered field due to the patch current is given by equations (8) and (9), and the electric field at the patch location $z = z'$ with the patch removed is obtained by using the laws of reflection and refraction to produce the following:

$$E_x^i = E_o\left[\frac{2j \sin(kz') \exp(jk_o d)}{\sqrt{\varepsilon_r}\cos(kd) + j \sin(kd)}\right] \tag{15}$$

By setting the total tangential electric field over the patch equal to zero, the following integral equations are obtained:

$$E_x^i = \frac{j\omega}{(2\pi)^2 k^2} \int_{-\infty}^{\infty}\int_{-\infty}^{\infty} [\zeta_{xx}(k_x,k_y,z')\, j_x(k_x,k_y) + \zeta_{yx}(k_x,k_y,z')\, j_y(k_x,k_y)] \exp(jk_x x + jk_y y)\, dk_x\, dk_y \tag{16}$$

$$E_y^i = \frac{j\omega}{(2\pi)^2 k^2} \int_{-\infty}^{\infty}\int_{-\infty}^{\infty} [\zeta_{xy}(k_x,k_y,z')\, j_x(k_x,k_y) + \zeta_{yy}(k_x,k_y,z')\, j_y(k_x,k_y)] \exp(jk_x x + jk_y y)\, dk_x\, dk_y \tag{17}$$

The integral equations (16) and (17) can be used to determine the patch current for a microstrip patch of any arbitrary shape. However, when one tries to solve equations (16) and (17) by the method of moments, it is difficult to arrive at a proper expansion function for the current distribution on the patch unless the geometry of the patch is an ordered shape such as a rectangle, a circle, or a square. It may be concluded that the application of equations (16) and (17) may be limited by complexity of the patch shape.

Radiation Pattern

The patch current obtained after solving equations (16) and (17) can be used to evaluate the radiation pattern. It is well known that the far field due to a radiating aperture is directly related to the Fourier transform of the tangential electric field over the aperture (ref. 9). Hence, the radiation pattern due to a microstrip patch embedded in a dielectric substrate with one surface grounded can be obtained from a knowledge of the Fourier transform of the electric field over the interface

between free space and the dielectric region. The transformed electric field in the plane of $z = d$ can be obtained from equations (8) and (9) as

$$e_x(k_x,k_y,z)\Big|_{z=d} = \frac{-j\omega\mu d}{k^2}\left[\zeta_{xx}(k_x,k_y)\, j_x(k_x,k_y) + \zeta_{yx}(k_x,k_y)\, j_y(k_x,k_y)\right] \tag{18}$$

$$e_y(k_x,k_y,z)\Big|_{z=d} = \frac{-j\omega\mu d}{k^2}\left[\zeta_{xy}(k_x,k_y)\, j_x(k_x,k_y) + \zeta_{yy}(k_x,k_y)\, j_y(k_x,k_y)\right] \tag{19}$$

where e_x and e_y are the Fourier transforms of E_x and E_y. The far field is then given by (ref. 9)

$$E_\theta = \left(e_x \cos\phi + e_y \sin\phi\right)\frac{jk_o}{2\pi r}\exp(-jk_o r) \tag{20}$$

$$E_\phi = \left(e_y \cos\phi - e_x \sin\phi\right)\cos\theta\,\frac{jk_o}{2\pi r}\exp(-jk_o r) \tag{21}$$

With the following coordinate transformation

$$k_x = k_o \cos\phi \sin\theta \tag{22a}$$

$$k_y = k_o \sin\phi \sin\theta \tag{22b}$$

the far-field radiation patterns become

$$E_\theta(\theta,\phi) = \frac{-k_o\omega\exp(-jk_o r)}{2\pi r k^2}\left\{\left[\zeta_{xx}(\theta,\phi)\cos\phi + \zeta_{xy}(\theta,\phi)\sin\phi\right] j_x(\theta,\phi) + \left[\zeta_{yx}(\theta,\phi)\cos\phi + \zeta_{yy}(\theta,\phi)\sin\phi\right] j_y(\theta,\phi)\right\} \tag{23}$$

$$E_\phi(\theta,\phi) = \left[\frac{-k_o\omega\exp(-jk_o r)}{2\pi r k^2}\right]\cos\theta\left\{\left[\zeta_{xy}(\theta,\phi)\cos\phi - \zeta_{xx}(\theta,\phi)\sin\phi\right] j_x(\theta,\phi) + \left[\zeta_{yy}(\theta,\phi)\cos\phi - \zeta_{yx}(\theta,\phi)\sin\phi\right] j_y(\theta,\phi)\right\} \tag{24}$$

where the quantities $\zeta_{xx}(\theta,\phi)$, $\zeta_{xy}(\theta,\phi)$, $\zeta_{yx}(\theta,\phi)$, and $\zeta_{yy}(\theta,\phi)$ are evaluated at $z = d$. Also, $j_x(\theta,\phi)$ and $j_y(\theta,\phi)$ are the Fourier transforms of the patch current with k_x and k_y replaced by equations (22).

After considerable mathematical manipulation, the radiation patterns can be written in the form

$$E_\theta(\theta,\phi) = C_o\left[j_x(\theta,\phi)\cos\phi + j_y(\theta,\phi)\sin\phi\right](\varepsilon_r - \sin^2\theta)\left\{\left(\frac{z'}{d} - 1\right)\left[\frac{\sin(D_k - Z_k')}{D_k - Z_k'}\right]\right.$$

$$+ \left[\frac{N_{TE}(\theta,\phi)}{D_{TE}(\theta,\phi)}\right]\left(\frac{\sin D_k}{D_k}\right) - j(\varepsilon_r - 1)\sin^2\theta \sin Z_k'$$

$$\left.\times \left[\frac{1}{D_{TE}(\theta,\phi)}\right]\left[\frac{1}{D_{TM}(\theta,\phi)}\right]\left(\frac{\sin D_k}{D_k}\right)\right\} \tag{25}$$

$$E_\phi(\theta,\phi) = -C_o\left[j_x(\theta,\phi)\sin\phi - j_y(\theta,\phi)\cos\phi\right](\varepsilon_r \cos\theta)$$

$$\times\left\{\left(\frac{z'}{d} - 1\right)\left[\frac{\sin(D_k - Z_k')}{D_k - Z_k'}\right] + \left[\frac{N_{TE}(\theta,\phi)}{D_{TE}(\theta,\phi)}\right]\left(\frac{\sin D_k}{D_k}\right)\right\} \tag{26}$$

where

$$N_{TE}(\theta,\phi) = \sqrt{\varepsilon_r - \sin^2\theta}\cos(D_k - Z_k') + j\cos\theta\sin(D_k - Z_k')$$

$$D_{TE}(\theta,\phi) = \sqrt{\varepsilon_r - \sin^2\theta}\cos D_k + j\cos\theta\sin D_k$$

$$D_{TM}(\theta,\phi) = \varepsilon_r\cos\theta\cos D_k + j\sqrt{\varepsilon_r - \sin^2\theta}\sin D_k$$

$$D_k = k_o d\sqrt{\varepsilon_r - \sin^2\theta}$$

$$Z_k' = k_o z'\sqrt{\varepsilon_r - \sin^2\theta}$$

$$C_o = \left(-\frac{\omega\mu k_o^2 d}{2\pi\varepsilon_r}\right)\left[\frac{\exp(-jk_o r)}{k_o r}\right]$$

Application to Rectangular Patch

Consider a microstrip antenna in the form of a rectangular patch with respective E- and H-plane dimensions of W_x and W_y, as shown in figure 2. The current distribution on the patch must be expanded in terms of eigenfunctions which satisfy the proper edge behavior such that the normal component of the patch current density is zero at the edge and the parallel component approaches infinity at the edge. In the classic eigenfunction solution of a problem involving edges, these edge conditions are explicitly used to select the eigenfunctions. However, it may be unnecessary here to use the exact eigenfunctions. Instead, one may expand the patch current density in terms of triangular, sinusoidal, or flat pulses to approximate the current distribution. Therefore, the rectangular patch is divided into rectangular subdomains which allow one to expand the current in terms of overlapping triangular pulses in the direction of the current and in terms of flat pulses orthogonal to the current. Hence,

$$J_x(x,y) = \sum_{m=1}^{M} \sum_{n=1}^{N+1} j_x^{mn} P_m(x) Q_n(y) \tag{27a}$$

$$J_y(x,y) = \sum_{m=1}^{M+1} \sum_{n=1}^{N} j_y^{mn} Q_m(x) P_n(y) \tag{27b}$$

where

$$P_m(x) = 1 + (x - x_m)/\Delta x \qquad \left((x_m - \Delta x) \leq x \leq x_m\right)$$

$$= 1 - (x - x_m)/\Delta x \qquad \left(x_m \leq x \leq (x_m + \Delta x)\right)$$

$$= 0$$

$$Q_n(y) = 1 \qquad \left(y_n \leq y \leq (y_n - \Delta y)\right)$$

$$= 0$$

$$\Delta x = W_x/(M + 1)$$

$$\Delta y = W_y/(N + 1)$$

and j_x^{mn} and j_y^{mn} are the unknown complex x- and y-directed current coefficients for the m,n subdomain.

With equation (7), the Fourier transforms of the patch current from equations (27) are

$$j_x(k_x,k_y) = \sum_{m=1}^{M} \sum_{n=1}^{N+1} j_x^{mn} F_{x,mn}(k_x,k_y) \tag{28a}$$

$$j_y(k_x,k_y) = \sum_{m=1}^{M+1} \sum_{n=1}^{N} j_y^{mn} F_{y,mn}(k_x,k_y) \tag{28b}$$

where

$$F_{x,mn}(k_x,k_y) = \int_{y_n-\Delta y}^{y_n} \int_{x_m-\Delta x}^{x_m+\Delta x} P_m(x)\, Q_n(y)\, \exp[-j(k_x x + k_y y)]\, dx\, dy$$

$$= \Delta x\, \Delta y \left[\frac{\sin(k_y \Delta y/2)}{k_y \Delta y/2}\right]\left[\frac{\sin(k_x \Delta x/2)}{k_x \Delta x/2}\right]^2$$

$$\times \exp\left[-jk_x x_m - jk_y y_n + jk_y(\Delta y/2)\right] \tag{29}$$

$$F_{y,mn}(k_x,k_y) = \int_{y_n-\Delta y}^{y_n+\Delta y} \int_{x_m-\Delta x}^{x_m} Q_m(x)\, P_n(y)\, \exp\left[-j(k_x x + k_y y)\right] dx\, dy$$

$$= \Delta x\, \Delta y \left[\frac{\sin(k_y \Delta y/2)}{k_y \Delta y/2}\right]^2\left[\frac{\sin(k_x \Delta x/2)}{k_x \Delta x/2}\right]$$

$$\times \exp\left[-jk_x x_m - jk_y y_n + jk_x(\Delta x/2)\right] \tag{30}$$

Substituting equations (28) into equations (16) and (17) results in the following integral equations:

$$E_x^i = \frac{j\omega}{(2\pi)^2 k^2}\left[\sum_{m=1}^{M}\sum_{n=1}^{N+1} j_x^{mn} \int_{-\infty}^{\infty}\int_{-\infty}^{\infty} \zeta_{xx}(k_x,k_y,z') \, F_{x,mn}(k_x,k_y)\right.$$

$$\times \exp(jk_x x + jk_y y)\, dk_x\, dk_y + \sum_{m=1}^{M+1}\sum_{n=1}^{N} j_y^{mn} \int_{-\infty}^{\infty}\int_{-\infty}^{\infty} \zeta_{yx}(k_x,k_y,z')$$

$$\left.\times F_{y,mn}(k_x,k_y) \exp(jk_x x + jk_y y)\, dk_x\, dk_y\right] \tag{31}$$

$$E_y^i = \frac{j\omega}{(2\pi)^2 k^2}\left[\sum_{m=1}^{M}\sum_{n=1}^{N+1} j_x^{mn} \int_{-\infty}^{\infty}\int_{-\infty}^{\infty} \zeta_{xy}(k_x,k_y,z') \, F_{x,mn}(k_x,k_y)\right.$$

$$\times \exp(jk_x x + jk_y y)\, dk_x\, dk_y + \sum_{m=1}^{M+1}\sum_{n=1}^{N} j_y^{mn} \int_{-\infty}^{\infty}\int_{-\infty}^{\infty} \zeta_{yy}(k_x,k_y,z')$$

$$\left.\times F_{y,mn}(k_x,k_y) \exp(jk_x x + jk_y y)\, dk_x\, dk_y\right] \tag{32}$$

If the method of moments is used with testing functions identical to the expansion functions, equations (31) and (32) can be reduced to algebraic equations. Multiplying equation (31) by $P_p(x)\, Q_q(y)$ and integrating with respect to x and y gives

$$E_{x,pq} = \sum_{m=1}^{M}\sum_{n=1}^{N+1} j_x^{mn} Z_{xx}^{pq,mn} + \sum_{m=1}^{M+1}\sum_{n=1}^{N} j_y^{mn} Z_{xy}^{pq,mn} \tag{33}$$

Likewise, multiplying equation (32) by $P_q(y)\, Q_p(x)$ and integrating gives

$$E_{y,pq} = \sum_{m=1}^{M}\sum_{n=1}^{N+1} j_x^{mn} Z_{yx}^{pq,mn} + \sum_{m=1}^{M+1}\sum_{n=1}^{N} j_y^{mn} Z_{yy}^{pq,mn} \tag{34}$$

where

$$E_{x,pq} = \int_{y_q-\Delta y}^{y_q} \int_{x_p-\Delta x}^{x_p+\Delta x} E_x^i \, P_p(x) \, Q_q(y) \, dx \, dy \tag{35}$$

$$E_{y,pq} = \int_{y_q-\Delta y}^{y_q+\Delta y} \int_{x_p-\Delta x}^{x_p} E_y^i \, P_q(y) \, Q_p(x) \, dx \, dy \tag{36}$$

$$Z_{xx}^{mn,pq} = \frac{j\omega}{(2\pi)^2 k^2} \int_{-\infty}^{\infty} \int_{-\infty}^{\infty} \zeta_{xx}(k_x,k_y,z') \, F_{x,mn}(k_x,k_y) \, F_{x,pq}(-k_x,-k_y) \, dk_x \, dk_y \tag{37}$$

$$Z_{xy}^{mn,pq} = \frac{j\omega}{(2\pi)^2 k^2} \int_{-\infty}^{\infty} \int_{-\infty}^{\infty} \zeta_{yx}(k_x,k_y,z') \, F_{y,mn}(k_x,k_y) \, F_{x,pq}(-k_x,-k_y) \, dk_x \, dk_y \tag{38}$$

$$Z_{yx}^{mn,pq} = \frac{j\omega}{(2\pi)^2 k^2} \int_{-\infty}^{\infty} \int_{-\infty}^{\infty} \zeta_{xy}(k_x,k_y,z') \, F_{x,mn}(k_x,k_y) \, F_{y,pq}(-k_x,-k_y) \, dk_x \, dk_y \tag{39}$$

$$Z_{yy}^{mn,pq} = \frac{j\omega}{(2\pi)^2 k^2} \int_{-\infty}^{\infty} \int_{-\infty}^{\infty} \zeta_{yy}(k_x,k_y) \, F_{y,mn}(k_x,k_y) \, F_{y,pq}(-k_x,-k_y) \, dk_x \, dk_y \tag{40}$$

By varying $p = 1, 2, \ldots, M$ and $q = 1, 2, \ldots, N + 1$ in equation (33) and by varying $p = 1, 2, \ldots, M + 1$ and $q = 1, 2, \ldots, N$ in equation (34), $M(N + 1) + (M + 1)N$ equations with $M(N + 1) + (M + 1)N$ unknowns are obtained. Hence, equations (33) and (34) can be written in the following matrix form, where the dimensions of each submatrix are given below the submatrix:

$$\begin{bmatrix} \underset{M(N+1)\times 1}{\left[E_{x,pq}\right]} \\ \hline \underset{(M+1)N\times 1}{\left[E_{y,pq}\right]} \end{bmatrix} = \begin{bmatrix} \underset{M(N+1)\times M(N+1)}{\left[Z_{xx}^{mn,pq}\right]} & \vdots & \underset{M(N+1)\times (M+1)N}{\left[Z_{xy}^{mn,pq}\right]} \\ \hline \underset{(M+1)N\times M(N+1)}{\left[Z_{yx}^{mn,pq}\right]} & \vdots & \underset{(M+1)N\times (M+1)N}{\left[Z_{yy}^{mn,pq}\right]} \end{bmatrix} \begin{bmatrix} \underset{M(N+1)\times 1}{\left[j_x^{mn}\right]} \\ \hline \underset{(M+1)N\times 1}{\left[j_y^{mn}\right]} \end{bmatrix} \tag{41}$$

With the variables changed such that $k_x = k_o\beta \cos\alpha$ and $k_y = k_o\beta \sin\alpha$, the generalized impedance elements in equation (41) are given by

$$Z_{xx}^{mn,pq} = C \int_{\beta=0}^{\infty} \int_{\alpha=0}^{\pi/2} b(\alpha,\beta) \left[\frac{\sin\left(\frac{1}{2} k_o\beta\, \Delta x \cos\alpha\right)}{\frac{1}{2} k_o\beta\, \Delta x \cos\alpha} \right]^2$$

$$\times \left[(\varepsilon_r - \beta^2 \cos^2\alpha)\, \xi_1(\beta) - j(\varepsilon_r - 1)\beta^2 \cos^2\alpha\, \xi_2(\beta)\right]$$

$$\times \cos\left[k_o\beta(x_m - x_p) \cos\alpha\right] \cos\left[k_o\beta(y_n - y_q) \sin\alpha\right] \beta\, d\beta\, d\alpha \qquad (42)$$

$$Z_{xy}^{mn,pq} = C \int_{\beta=0}^{\infty} \int_{\alpha=0}^{\pi/2} b(\alpha,\beta) \left[\frac{\sin\left(\frac{1}{2} k_o\beta\, \Delta x \cos\alpha\right)}{\frac{1}{2} k_o\beta\, \Delta x \cos\alpha} \right] \left[\frac{\sin\left(\frac{1}{2} k_o\beta\, \Delta y \sin\alpha\right)}{\frac{1}{2} k_o\beta\, \Delta y \sin\alpha} \right]$$

$$\times \left[\xi_1(\beta) + j(\varepsilon_r - 1)\, \xi_2(\beta)\right]\beta^2 \sin\alpha \cos\alpha$$

$$\times \sin\left[k_o\beta\left(x_m - x_p + \frac{\Delta x}{2}\right) \cos\alpha\right] \sin\left[k_o\beta\left(y_n - y_q + \frac{\Delta y}{2}\right) \sin\alpha\right] \beta\, d\beta\, d\alpha \qquad (43)$$

$$Z_{yx}^{mn,pq} = Z_{xy}^{pq,mn} \qquad (44)$$

$$Z_{yy}^{mn,pq} = C \int_{\beta=0}^{\infty} \int_{\alpha=0}^{\pi/2} b(\alpha,\beta) \left[\frac{\sin\left(\frac{1}{2} k_o\beta\, \Delta y \sin\alpha\right)}{\frac{1}{2} k_o\beta\, \Delta y \sin\alpha} \right]^2$$

$$\times \left[(\varepsilon_r - \beta^2 \sin^2\alpha)\, \xi_1(\beta) - j(\varepsilon_r - 1)\beta^2 \sin^2\alpha\, \xi_2(\beta)\right]$$

$$\times \sin\left[k_o\beta(x_m - x_p) \cos\alpha\right] \sin\left[k_o\beta(y_n - y_q) \sin\alpha\right] \beta\, d\beta\, d\alpha \qquad (45)$$

where

$$C = \frac{j120}{\pi\varepsilon_r} (k_o z')(k_o\, \Delta x)(k_o\, \Delta y) \qquad (46)$$

$$b(\alpha,\beta) = \left[\frac{\sin\left(\frac{1}{2}\, k_o \beta\, \Delta x \cos\alpha\right)}{\frac{1}{2}\, k_o \beta\, \Delta x \cos\alpha}\right]\left[\frac{\sin\left(\frac{1}{2}\, k_o \beta\, \Delta y \sin\alpha\right)}{\frac{1}{2}\, k_o \beta\, \Delta y \sin\alpha}\right] \tag{47}$$

$$\xi_1(\beta) = \left[\frac{\sin\left(k_o z' \sqrt{\varepsilon_r - \beta^2}\right)}{k_o z' \sqrt{\varepsilon_r - \beta^2}}\right] \times \left\{\frac{j\sqrt{1-\beta^2}\, \sin\left[k_o(d-z')\sqrt{\varepsilon_r - \beta^2}\right] + \sqrt{\varepsilon_r - \beta^2}\, \cos\left[k_o(d-z')\sqrt{\varepsilon_r - \beta^2}\right]}{j\sqrt{1-\beta^2}\, \sin\left(k_o d\sqrt{\varepsilon_r - \beta^2}\right) + \sqrt{\varepsilon_r - \beta^2}\, \cos\left(k_o d\sqrt{\varepsilon_r - \beta^2}\right)}\right\} \tag{48}$$

$$\xi_2(\beta) = \left[\frac{\sin\left(k_o z' \sqrt{\varepsilon_r - \beta^2}\right) \Big/ \left(k_o z' \sqrt{\varepsilon_r - \beta^2}\right)}{j\sqrt{\varepsilon_r - \beta^2}\, \sin\left(k_o d\sqrt{\varepsilon_r - \beta^2}\right) + \varepsilon_r \sqrt{1-\beta^2}\, \cos\left(k_o d\sqrt{\varepsilon_r - \beta^2}\right)}\right] \times \left[\frac{\left(\varepsilon_r - \beta^2\right) \sin\left(k_o z' \sqrt{\varepsilon_r - \beta^2}\right)}{j\sqrt{1-\beta^2}\, \sin\left(k_o d\sqrt{\varepsilon_r - \beta^2}\right) + \sqrt{\varepsilon_r - \beta^2}\, \cos\left(k_o d\sqrt{\varepsilon_r - \beta^2}\right)}\right] \tag{49}$$

and the integration over the k_x, k_y-plane has been reduced to an integration over one quadrant by using the even and odd properties of the integrand.

The impedance elements are computed by using numerical integration techniques and properly accounting for the contribution of surface wave poles. The unknown complex current coefficients j_x^{mn} and j_y^{mn} are then determined from equation (41) by using matrix inversion.

Patch Current Distribution

The patch current distribution can be obtained by solving the matrix equation (41). The matrix elements are numerically computed by using the Gauss quadrature numerical integration technique. For accurate computation, the upper limit on the β integration must be terminated at a sufficiently large value. It was found numerically that any increase in the upper limit above 600 does not change the values of the matrix elements appreciably.

Without loss of generality, the left-hand side of equation (41) may be assumed to be unity. Therefore, the numerical results for patch current distribution given in this report are normalized to the total incident electric field on the patch, that is, E_x^i given in equation (15).

Although the problem of the rectangular microstrip antenna is formulated correctly in terms of coupled integral equations, the approximation to the patch current distribution is introduced when one tries to solve the integral equations by the method of moments or by Galerkin's method. The numerical solution of equation (41) is expected to converge when the number of subdomains approaches infinity. In practice, however, because of computer storage and time limitations, it is desirable to obtain an answer with as few subdomains as possible. It is, therefore, important to know the proper number of subdomains to obtain accurate values of the patch current distribution.

For a $1.0\lambda_\varepsilon$ square patch ($W_x = W_y$) in free space and illuminated by a plane wave at normal incidence, the patch current converges to the correct value when $M \geq 7$ and also $N \geq 7$ (ref. 10). The present problem becomes identical to the one in reference 10 when $d = \infty$ and $\varepsilon_r = 1$. It is expected that the patch current obtained after solving equation (41) for $M \geq 7$ and $N \geq 7$ will oscillate about the converged value of the patch current in reference 10 as the substrate thickness d is varied. The patch current at the center of the patch obtained after solving equation (41) for $M = N = 7$ is plotted in figure 3 as a function of the substrate thickness for a dielectric constant of unity. As expected, both the real and imaginary parts of the patch current indeed oscillate about the free space value. For further calculations, the number of subdomains is selected such that $M = N = 11$.

For further verification of the present method, it is important to check the results obtained with the present method with earlier known results. The transverse-electric-strip (TE-strip) problem is a limiting case of the rectangular patch under the condition $W_y \to \infty$. The patch current at the center, therefore, must asymptotically approach the TE-strip current (refs. 11 and 12) as W_y approaches infinity. Figure 4 shows the results are as expected.

After checking the validity of the present formulation, equation (41) is solved for a square patch. For x-polarized plane wave excitation, the magnitude of the y-directed current is very small compared with the magnitude of the x-directed current (typically 25 to 30 dB less); therefore, J_y may be neglected. It is advantageous to study the current distribution on the patch, $J_x(x,y)$, which may allow one to express the current in terms of more appropriate basis functions. The current distribution $J_x(x,y)$, obtained after solving equation (41), is plotted in figure 5 as a function of x at $y = W_y/2$ and as a function of y at $x = W_x/2$. It is clear from figure 5 that $J_x(x,y)$ is almost sinusoidal in the direction of the current and is uniform, except at the edges, along the direction orthogonal to the current; therefore, it is more appropriate and advantageous to express the patch current density in the following form:

$$J_x(x,y) = j_x \cos(\pi x/W_x) \tag{50}$$

The assumption of uniform distribution in the y direction gives a value of j_x slightly higher than the true value. With the above current distribution, the number of unknowns to be evaluated is reduced from $M(N + 1) + (M + 1)N$ to 1. The matrix equation (41) then reduces to

$$E_x^i = Z_{xx} j_x \tag{51}$$

where

$$Z_{xx} = \frac{\pi}{2} C \int_{\beta=0}^{\infty} \int_{\alpha=0}^{\pi/2} \left[\frac{\sin\left(\frac{1}{2} k_o \beta W_y \sin \alpha\right)}{\frac{1}{2} k_o \beta W_y \sin \alpha} \right]^2 \left[\frac{2\pi \cos\left(\frac{1}{2} k_o \beta W_x \cos \alpha\right)}{\pi^2 - (k_o \beta W_x \cos \alpha)^2} \right]^2$$

$$\times \left[(\varepsilon_r - \beta^2 \cos^2\alpha)\, \xi_1(\beta) - j(\varepsilon_r - 1)\beta^2 \cos^2\alpha\, \xi_2(\beta) \right] \beta \, d\beta \, d\alpha \qquad (52)$$

and C, $\xi_1(\beta)$, and $\xi_2(\beta)$ are given by equations (46), (48), and (49).

RESULTS

Patch Resonance

It is informative to plot the real and imaginary parts of j_x as a function of the E-plane dimension, as shown in figure 6. The plot has the characteristic resonant behavior of a tuned circuit and can be used to predict the resonant width (i.e., the resonant frequency) of a rectangular microstrip antenna. The resonant frequency can be defined as the frequency at which the imaginary part of j_x is zero. With the above criteria, the resonant frequency of a rectangular patch is determined and plotted as a function of the H-plane dimension in figure 7 along with available theoretical and experimental results from reference 4. It should be noted that the theoretical prediction of resonant frequency using the cavity model (ref. 4) requires a semiempirical correction. However, the present method of analysis, without any correction, predicts the resonant frequency within the tolerance limits of the dielectric constant ($\varepsilon_r = 2.62 \pm 0.02$).

Resonant Width

With the resonant criteria defined in the previous section, the resonant width of a rectangular microstrip patch is computed as a function of dielectric substrate thickness for the aspect ratios W_y/W_x of 0.5, 1.0, and 1.5 and for dielectric constants ε_r of 1.0, 2.5, 6.0, and 10.0. The values are presented in figures 8 to 11. These calculations show that the resonant width (normalized to the dielectric wavelength) of a rectangular microstrip patch antenna generally increases with increases in the dielectric constant of the substrate and decreases with increases in the substrate thickness.

The resonant width of a rectangular patch is also plotted in figure 12 as a function of the aspect ratio W_y/W_x. An increase in the aspect ratio causes a decrease in the resonant width of the patch. Under the limiting case of W_y/W_x being large, the resonant width of the rectangular patch will approach asymptotically the resonant width of the TE-strip (ref. 12).

It is informative to plot the resonant width of the rectangular patch for a thick dielectric substrate, as shown in figure 13. These calculations show the resonant width decreases approximately linearly with increases in substrate thickness

for $d < 0.06\lambda_\varepsilon$. For $d > 0.06\lambda_\varepsilon$, the curve is no longer linear and scaling can no longer be used to estimate the resonant frequency of a microstrip antenna.

In some applications it is desirable to cover the microstrip patch with a dielectric coating to protect the antenna from environmental conditions. The resonant width of a rectangular microstrip patch for various dielectric coating thicknesses is computed and is presented in figure 14. These calculations indicate that the resonant width decreases with an increase in the thickness of the coating.

Bandwidth

The bandwidth of microstrip antennas may be defined as the band of frequencies over which the input voltage standing-wave ratio (VSWR) in the feed line is less than a specified value (usually 2 or 3). Since the input impedance of a microstrip antenna is proportional to the patch current, the input impedance variation with frequency will be the same as that of the patch current. Hence, the input reflection coefficient variation with frequency can be calculated from a knowledge of the patch current density. Under the assumption of a unit voltage source and a perfect impedance match at resonance, the reflection coefficient Γ can be calculated from

$$\Gamma = \frac{j_x - j_{x,r}}{j_x + j_{x,r}} \tag{53}$$

where $j_{x,r}$ is the amplitude of the patch current density at resonance. The magnitude of the input reflection coefficient thus calculated is shown in figure 15 as a function of the patch size for a square patch. For the input VSWR in the feed line to be less than 3, the percent bandwidth may be obtained by

$$\text{Percent bandwidth} = \frac{100\ \Delta(W_x/\lambda_\varepsilon)_3}{(W_x/\lambda_\varepsilon)_o} \tag{54}$$

where $\Delta(W_x/\lambda_\varepsilon)_3$ and $(W_x/\lambda_\varepsilon)_o$ are defined in figure 15. The percent bandwidth for a VSWR less than 2 can be determined in a like manner. The percent bandwidth thus calculated is compared with measured data in figure 16 for probe-fed square patches. The apparent increase in the measured percent bandwidth may be due to feed-connection insertion loss and copper loss in the experimental models. The calculated percent bandwidths for rectangular patches are presented in figures 17 to 22 for aspect ratios W_y/W_x of 0.5, 1.0, and 1.5 and dielectric constants ε_r of 1.0, 2.5, and 6.0. These calculations show an increase in bandwidth with increases in dielectric substrate thickness, which is consistent with previous measured results (ref. 13).

The percent bandwidth of a square microstrip patch with a thicker dielectric substrate is presented in figure 23. This calculation indicates that a bandwidth up to 20 percent may be possible by constructing the antenna on a thick dielectric.

Figure 24 shows the effect of a dielectric coating on the percent bandwidth of a square patch. The calculations show no appreciable change in percent bandwidth when

the cover thickness is less than $0.04\lambda_\varepsilon$. However, for thicker dielectric coatings (greater than $0.04\lambda_\varepsilon$), there is an increase in the bandwidth of about 1 percent.

Radiation Pattern

With the x-directed current distribution given in equation (51), the radiation patterns of a rectangular microstrip antenna are computed from equations (25) and (26). The results are presented in figures 25 and 26 along with experimental data (ref. 4). There is a close agreement between the calculated and measured radiation patterns.

CONCLUSION

The dyadic Green's function for a current source located in a dielectric with one surface grounded has been derived. The dyadic Green's function was used to arrive at a set of coupled electric-field integral equations for a microstrip patch of arbitrary shape. As an example of the applicability to microstrip antennas, the integral equations were solved for a rectangular patch using Galerkin's method. It is shown that the patch current can be used to accurately predict the resonant frequency, the bandwidth, and the radiation patterns of microstrip antennas. Data for a range of design parameters are presented for the rectangular microstrip antenna.

Langley Research Center
National Aeronautics and Space Administration
Hampton, VA 23665
January 25, 1984

APPENDIX

DERIVATION OF DYADIC GREEN'S FUNCTION

The expression in equation (5) must satisfy the wave equations (3) and (4); therefore,

$$\nabla^2 \bar{\bar{G}}^{I}(x,y,z,x',y',z') + k^2\, \bar{\bar{G}}^{I}(x,y,z,x',y',z') = -\mu \bar{\bar{I}}\, \delta(x-x')\, \delta(y-y')\, \delta(z-z') \tag{A1}$$

$$\nabla^2 \bar{\bar{G}}^{II}(x,y,z,x',y',z') + k_o^2\, \bar{\bar{G}}^{II}(x,y,z,x',y',z') = 0 \tag{A2}$$

It is clear from equations (A1) and (A2) that the Green's function is the electric vector potential due to a unit impulse current located at the point (x',y',z').

It is advantageous and less tedious to obtain the solution of equations (A1) and (A2) in the spectral domain. Therefore, taking the bidimensional Fourier transform of both sides of equations (A1) and (A2) and using Sommerfeld's radiation condition (ref. 14) yields

$$\frac{\partial^2 \bar{\bar{g}}^{I}(k_x,k_y,z,x',y',z')}{\partial z^2} + \left(k^{I}\right)^2\, \bar{\bar{g}}^{I}(k_x,k_y,z,x',y',z')$$

$$= -\mu \bar{\bar{I}}\, \delta(z-z') \exp\left[-j(k_x x' + k_y y')\right] \tag{A3}$$

$$\frac{\partial^2 \bar{\bar{g}}^{II}(k_x,k_y,z,x',y',z')}{\partial z^2} + \left(k^{II}\right)^2\, \bar{\bar{g}}^{II}(k_x,k_y,z,x',y',z') = 0 \tag{A4}$$

where

$$\bar{\bar{g}}^{I/II}(k_x,k_y,z,x',y',z') = \int_{-\infty}^{\infty} \int_{-\infty}^{\infty} \bar{\bar{G}}^{I/II}(x,y,z,x',y',z') \exp\left[-j(k_x x + k_y y)\right] dx\, dy \tag{A5}$$

$$k^{I} = \sqrt{k_o^2 \varepsilon_r - \left(k_x^2 + k_y^2\right)} \qquad \left(k_o^2 \varepsilon_r > \left(k_x^2 + k_y^2\right)\right) \tag{A6a}$$

$$= -j\sqrt{\left(k_x^2 + k_y^2\right) - k_o^2 \varepsilon_r} \qquad \left(k_o^2 \varepsilon_r < \left(k_x^2 + k_y^2\right)\right) \tag{A6b}$$

$$k^{II} = \sqrt{k_o^2 - (k_x^2 + k_y^2)} \qquad (k_o^2 > (k_x^2 + k_y^2)) \tag{A7a}$$

$$= -j\sqrt{(k_x^2 + k_y^2) - k_o^2} \qquad (k_o^2 < (k_x^2 + k_y^2)) \tag{A7b}$$

With a shortened notation $\bar{\bar{g}}^{I/II}$, $\bar{\bar{g}}^{I/II}(k_x,k_y,z,x',y',z')$ may be expressed as

$$\bar{\bar{g}}^{I/II} = \bar{g}_x^{I/II}\hat{x} + \bar{g}_y^{I/II}\hat{y} + \bar{g}_z^{I/II}\hat{z} \tag{A8}$$

where

$$\bar{g}_x^{I/II} = g_{xx}^{I/II}\hat{x} + g_{yx}^{I/II}\hat{y} + g_{zx}^{I/II}\hat{z} \tag{A9}$$

$$\bar{g}_y^{I/II} = g_{xy}^{I/II}\hat{x} + g_{yy}^{I/II}\hat{y} + g_{zy}^{I/II}\hat{z} \tag{A10}$$

$$\bar{g}_z^{I/II} = g_{xz}^{I/II}\hat{x} + g_{yz}^{I/II}\hat{y} + g_{zz}^{I/II}\hat{z} \tag{A11}$$

The scalar components of $\bar{\bar{g}}^{I/II}$ satisfy the following wave equations:

$$\frac{\partial^2 g_{xx}^I}{\partial z^2} + (k^I)^2 g_{xx}^I = -\mu\,\delta(z-z')\exp[-j(k_x x' + k_y y')] \tag{A12}$$

$$\frac{\partial^2 g_{yy}^I}{\partial z^2} + (k^I)^2 g_{yy}^I = -\mu\,\delta(z-z')\exp[-j(k_x x' + k_y y')] \tag{A13}$$

$$\frac{\partial^2 g_{zz}^I}{\partial z^2} + (k^I)^2 g_{zz}^I = -\mu\,\delta(z-z')\exp[-j(k_x x' + k_y y')] \tag{A14}$$

Other components satisfy the following equations for regions I and II:

$$\frac{\partial^2 f^I}{\partial z^2} + \left(k^I\right)^2 f^I = 0 \tag{A15}$$

$$\frac{\partial^2 f^{II}}{\partial z^2} + \left(k^{II}\right)^2 f^{II} = 0 \tag{A16}$$

where f^I denotes the right-hand scalar components of equations (A9) to (A11) (excluding g^I_{xx}, g^I_{yy}, and g^I_{zz} for region I, and f^{II} denotes the right-hand scalar components of equations (A9) to (A11) for region II.

The solution of equation (A12) has two parts, complementary and particular. The complementary solution can be written in the form

$$g^I_{xxc} = C^+_{xx} \exp(-jk^I z) + C^-_{xx} \exp(jk^I z) \tag{A17}$$

where C^+_{xx} and C^-_{xx} are unknown constants. For the particular solution, the Fourier transform of both sides of equation (A12) is taken with respect to z and yields

$$g^I_{xxp}(k_x,k_y,k_z,x',y',z') = \frac{\mu \exp\left[-j(k_x x' + k_y y' + k_z z')\right]}{k_z^2 - \left(k^I\right)^2} \tag{A18}$$

Taking the inverse transform with respect to z yields

$$g^I_{xxp}(k_x,k_y,z,x',y',z') = \frac{\mu \exp\left[-j(k_x x' + k_y y')\right]}{2\pi} \int_{-\infty}^{\infty} \frac{\exp\left[jk_z(z - z')\right]}{k_z^2 - (k^I)^2}\, dk_z \tag{A19}$$

The integrand in equation (A19) has poles at $k_z = \pm k^I$; therefore, equation (A19) can be evaluated through contour integration in the complex domain. Hence,

$$g^I_{xxp} = \frac{-j\mu}{2k^I} \exp\left[-j(k_x x' + k_y y')\right] \exp\left[-jk^I|(z - z')|\right] \tag{A20}$$

APPENDIX

The complete solution of equation (A12) can be obtained from equations (A17) and (A20) as

$$g^{I}_{xx} = C^{+}_{xx} \exp(-jk^{I}z) + C^{-}_{xx} \exp(jk^{I}z)$$

$$- \frac{j\mu}{2k^{I}} \exp[-j(k_x x' + k_y y')] \exp[-jk^{I}|(z - z')|] \qquad \text{(A21)}$$

Likewise, the solutions of equations (A13), (A14), (A15), and (A16) are obtained in the following forms:

$$g^{I}_{yy} = C^{+}_{yy} \exp(-jk^{I}z) + C^{-}_{yy} \exp(jk^{I}z)$$

$$- \frac{j\mu}{2k^{I}} \exp[-j(k_x x' + k_y y')] \exp[-jk^{I}|(z - z')|] \qquad \text{(A22)}$$

$$g^{I}_{zz} = C^{+}_{zz} \exp(-jk^{I}z) + C^{-}_{zz} \exp(jk^{I}z)$$

$$- \frac{j\mu}{2k^{I}} \exp[-j(k_x x' + k_y y')] \exp[-jk^{I}|(z - z')|] \qquad \text{(A23)}$$

$$f^{I} = C^{+} \exp(-jk^{I}z) + C^{-} \exp(jk^{I}z) \qquad \text{(A24)}$$

$$f^{II} = D^{+} \exp(-jk^{II}z) \qquad \text{(A25)}$$

where C^{+} and C^{-} are the coefficients of g^{I} excluding those given in equations (A21) to (A23), and D^{+} are the coefficients of g^{II}.

The unknown coefficients in equations (A21) to (A25) are evaluated by applying the boundary conditions on $\overline{\overline{g}}^{I/II}$. These boundary conditions are obtained by equating to zero the tangential electric field at the plane $z = 0$ and enforcing the continuity of tangential electric and magnetic fields at the plane $z = d$. The

APPENDIX

Fourier transforms of the electromagnetic fields in regions I and II may be obtained through the following relations:

$$\bar{h}^{I/II}(k_x,k_y,z,x',y',z') = \frac{1}{\mu}(\bar{K} \times \bar{\bar{g}}^{I/II}) \tag{A26}$$

$$\bar{e}^{I/II}(k_x,k_y,z,x',y',z') = -\frac{j\omega}{k^2}(\bar{K} \times \bar{K} \times \bar{\bar{g}}^{I/II}) \tag{A27}$$

where

$$\bar{K} = \hat{x}(jk_x) + \hat{y}(jk_y) + \hat{z}\left(\frac{\partial}{\partial z}\right) \tag{A28}$$

Subjecting the field obtained from equations (A26) and (A27) to the boundary conditions gives, for zero tangential electric field at $z = 0$,

$$g^I_{xx} = g^I_{xy} = g^I_{xz} = g^I_{yx} = g^I_{yy} = g^I_{yz} = 0 \tag{A29}$$

$$\frac{\partial g^I_{zx}}{\partial z} = \frac{\partial g^I_{zy}}{\partial z} = \frac{\partial g^I_{zz}}{\partial z} = 0 \tag{A30}$$

Continuity of the tangential magnetic field at $z = d$ yields

$$\frac{\partial g^I_{xx}}{\partial z} = \frac{\partial g^{II}_{xx}}{\partial z} \tag{A31}$$

$$\frac{\partial g^I_{xy}}{\partial z} = \frac{\partial g^{II}_{xy}}{\partial z} \tag{A32}$$

$$\frac{\partial g^I_{xz}}{\partial z} = \frac{\partial g^{II}_{xz}}{\partial z} \tag{A33}$$

$$\frac{\partial g^I_{yx}}{\partial z} = \frac{\partial g^{II}_{yx}}{\partial z} \tag{A34}$$

$$\frac{\partial g_{yy}^{I}}{\partial z} = \frac{\partial g_{yy}^{II}}{\partial z} \tag{A35}$$

$$\frac{\partial g_{yz}^{I}}{\partial z} = \frac{\partial g_{yz}^{II}}{\partial z} \tag{A36}$$

$$\frac{\partial g_{zx}^{I}}{\partial z} = \frac{\partial g_{zx}^{II}}{\partial z} \tag{A37}$$

$$\frac{\partial g_{zy}^{I}}{\partial z} = \frac{\partial g_{zy}^{II}}{\partial z} \tag{A38}$$

$$\frac{\partial g_{zz}^{I}}{\partial z} = \frac{\partial g_{zz}^{II}}{\partial z} \tag{A39}$$

$$g_{zx}^{I} = g_{zx}^{II} \tag{A40}$$

$$g_{zy}^{I} = g_{zy}^{II} \tag{A41}$$

$$g_{zz}^{I} = g_{zz}^{II} \tag{A42}$$

Continuity of the tangential electric field at $z = d$ yields

$$g_{xx}^{I} = g_{xx}^{II} \tag{A43}$$

$$g_{xy}^{I} = g_{xy}^{II} \tag{A44}$$

$$g_{xz}^{I} = g_{xz}^{II} \tag{A45}$$

$$g_{yx}^{I} = g_{yx}^{II} \tag{A46}$$

$$g_{yy}^{I} = g_{yy}^{II} \tag{A47}$$

$$g^{I}_{yz} = g^{II}_{yz} \tag{A48}$$

$$k_x(\varepsilon_r - 1)g^{I}_{xy} + k_y(\varepsilon_r - 1)g^{I}_{yy} = j\left(\varepsilon_r \frac{\partial g^{II}_{zy}}{\partial z} - \frac{\partial g^{I}_{zy}}{\partial z}\right) \tag{A49}$$

$$k_y(\varepsilon_r - 1)g^{I}_{yx} + k_x(\varepsilon_r - 1)g^{I}_{xx} = j\left(\varepsilon_r \frac{\partial g^{II}_{zx}}{\partial z} - \frac{\partial g^{I}_{zx}}{\partial z}\right) \tag{A50}$$

$$k_y(\varepsilon_r - 1)g^{I}_{yz} + k_x(\varepsilon_r - 1)g^{I}_{xz} = j\left(\varepsilon_r \frac{\partial g^{II}_{zz}}{\partial z} - \frac{\partial g^{I}_{zz}}{\partial z}\right) \tag{A51}$$

Subjecting equations (A21) to (A25) to the conditions given by equations (A29) to (A51) and solving the set of simultaneous equations for C^+ and C^- results in

$$g^{I}_{xx} = f^{I}_{xx} \exp\left[-j(k_x x' + k_y y')\right] \tag{A52}$$

$$g^{I}_{yy} = f^{I}_{yy} \exp\left[-j(k_x x' + k_y y')\right] \tag{A53}$$

$$g^{I}_{zz} = f^{I}_{zz} \exp\left[-j(k_x x' + k_y y')\right] \tag{A54}$$

$$g^{I}_{zx} = f^{I}_{zx} k_x \exp\left[-j(k_x x' + k_y y')\right] \tag{A55}$$

$$g^{I}_{zy} = f^{I}_{zy} k_y \exp\left[-j(k_x x' + k_y y')\right] \tag{A56}$$

where, for $(z - z') < 0$,

$$f^{I}_{xx} = f^{I}_{yy} = \mu z \left[\frac{k^I \cos k^I(d - z') + jk^{II} \sin k^I(d - z')}{k^I \cos(k^I d) + jk^{II} \sin(k^I d)}\right]\left[\frac{\sin(k^I z)}{k^I z}\right] \tag{A57}$$

$$f^{I}_{zz} = -\frac{j\mu}{k^I}\left[\frac{k^I \cos k^I(d - z') + jk^{II}\varepsilon_r \sin k^I(d - z')}{k^{II}\varepsilon_r \cos(k^I d) + jk^I \sin(k^I d)}\right]\left[\cos(k^I z)\right] \tag{A58}$$

or, for $(z - z') > 0$,

$$f_{xx}^{I} = f_{yy}^{I} = -\mu z\left[\frac{\sin k^{I}(z - z')}{k^{I}z}\right] + \mu z\left[\frac{k^{I}\cos k^{I}(d - z') + jk^{II}\sin k^{I}(d - z')}{k^{I}\cos(k^{I}d) + jk^{II}\sin(k^{I}d)}\right]\left[\frac{\sin(k^{I}z)}{k^{I}z}\right] \tag{A59}$$

$$f_{zz}^{I} = -\mu z\left[\frac{\sin k^{I}(z - z')}{k^{I}z}\right] - \frac{j\mu}{k^{I}}\left[\frac{k^{I}\cos k^{I}(d - z') + jk^{II}\varepsilon_{r}\sin k^{I}(d - z')}{k^{II}\varepsilon_{r}\cos(k^{I}d) + jk^{I}\sin(k^{I}d)}\right]\left[\cos(k^{I}z)\right] \tag{A60}$$

Also,

$$f_{zx}^{I} = f_{zy}^{I} = \frac{\mu(\varepsilon_{r} - 1)\sin(k^{I}z')\cos(k^{I}z)}{[k^{I}\cos(k^{I}d) + jk^{II}\sin(k^{I}d)][k^{II}\varepsilon_{r}\cos(k^{I}d) + jk^{I}\sin(k^{I}d)]} \tag{A61}$$

The other components of $\overline{\overline{g}}^{I}$ are zero. Likewise, the components of $\overline{\overline{g}}^{II}$ are given by

$$g_{xx}^{II} = f_{xx}^{II}\exp[-j(k_{x}x' + k_{y}y')]\exp[-jk^{II}(z - d)] \tag{A62}$$

$$g_{yy}^{II} = f_{yy}^{II}\exp[-j(k_{x}x' + k_{y}y')]\exp[-jk^{II}(z - d)] \tag{A63}$$

$$g_{zz}^{II} = f_{zz}^{II}\exp[-j(k_{x}x' + k_{y}y')]\exp[-jk^{II}(z - d)] \tag{A64}$$

$$g_{zx}^{II} = f_{zx}^{II}k_{x}\exp[-j(k_{x}x' + k_{y}y')]\exp[-jk^{II}(z - d)] \tag{A65}$$

$$g_{zy}^{II} = f_{zy}^{II}k_{y}\exp[-j(k_{x}x' + k_{y}y')]\exp[-jk^{II}(z - d)] \tag{A66}$$

where

$$f_{xx}^{II} = f_{yy}^{II} = \left[\frac{\mu \sin(k^I z')}{k^I \cos(k^I d) + jk^{II} \sin(k^I d)}\right] \tag{A67}$$

$$f_{zz}^{II} = -\mu(d - z')\left[\frac{\sin k^I(d - z')}{k^I(d - z')}\right]$$

$$- \frac{j\mu}{k^I}\left[\frac{k^I \cos k^I(d - z') + jk^{II}\varepsilon_r \sin k^I(d - z')}{k^{II}\varepsilon_r \cos(k^I d) + jk^I \sin(k^I d)}\right]\left[\cos(k^I d)\right] \tag{A68}$$

$$f_{zx}^{II} = f_{zy}^{II} = \frac{\mu(\varepsilon_r - 1) \sin(k^I z') \cos(k^I d)}{\left[k^I \cos(k^I d) + jk^{II} \sin(k^I d)\right]\left[k^{II}\varepsilon_r \cos(k^I d) + jk^I \sin(k^I d)\right]} \tag{A69}$$

The other components of $\bar{\bar{g}}^{II}$ are zero.

With the inverse Fourier transform, the dyadic Green's function for regions I and II is obtained from

$$\bar{\bar{G}}^I(x,y,z,x',y',z') = \left(\frac{1}{2\pi}\right)^2 \int_{-\infty}^{\infty}\int_{-\infty}^{\infty} \bar{\bar{g}}^I(k_x,k_y,z,x',y',z') \exp\left[j(k_x x + k_y y)\right] dk_x\, dk_y \tag{A70}$$

$$\bar{\bar{G}}^{II}(x,y,z,x',y',z') = \left(\frac{1}{2\pi}\right)^2 \int_{-\infty}^{\infty}\int_{-\infty}^{\infty} \bar{\bar{g}}^{II}(k_x,k_y,z,x',y',z') \exp\left[j(k_x x + k_y y)\right] dk_x\, dk_y \tag{A71}$$

REFERENCES

1. Carver, Keith R.; and Mink, James W.: Microstrip Antenna Technology. IEEE Trans. Antennas & Propag., vol. AP-29, no. 1, Jan. 1981, pp. 2-24.

2. Derneryd, Anders G.: Linearly Polarized Microstrip Antennas. IEEE Trans. Antennas & Propag., vol. AP-24, no. 6, Nov. 1976, pp. 846-851.

3. Derneryd, Anders G.: A Theoretical Investigation of the Rectangular Microstrip Antenna Element. IEEE Trans. Antennas & Propag., vol. AP-26, no. 4, July 1978, pp. 532-535.

4. Lo, Y. T.; Solomon, D.; and Richards, W. F.: Theory and Experiment on Microstrip Antennas. IEEE Trans. Antennas & Propag., vol. AP-27, no. 2, Mar. 1979, pp. 137-145.

5. Agrawal, Pradeep K.; and Bailey, M. C.: An Analysis Technique for Microstrip Antennas. IEEE Trans. Antennas & Propag., vol. AP-25, no. 6, Nov. 1977, pp. 756-759.

6. Newman, Edward H.; and Tulyathan, Pravit: Analysis of Microstrip Antennas Using Moment Methods. IEEE Trans. Antennas & Propag., vol. AP-29, no. 1, Jan. 1981, pp. 47-53.

7. Itoh, Tatsuo; and Menzel, Wolfgang: A Full-Wave Analysis Method for Open Microstrip Structures. IEEE Trans. Antennas & Propag., vol. AP-29, no. 1, Jan. 1981, pp. 63-68.

8. Araki, Kiyomichi; and Itoh, Tatsuo: Hankel Transform Domain Analysis of Open Circular Microstrip Radiating Structures. IEEE Trans. Antennas & Propag., vol. AP-29, no. 1, Jan. 1981, pp. 84-89.

9. Collin, Robert E.; and Zucker, Francis J.: Antenna Theory. Part 1. McGraw-Hill Book Co., Inc., c.1969.

10. Glisson, Allen Wilburn, Jr.: On the Development of Numerical Techniques for Treating Arbitrarily-Shaped Surfaces. Ph. D. Diss., Univ. of Mississippi, June 1978.

11. Bailey, M. C.: Analysis of the Properties of Microstrip Antennas Using Strips Embedded in a Grounded Dielectric Slab. 1979 International Symposium Digest - Antennas and Propagation - Volume I, IEEE, 1979, pp. 370-373.

12. Bailey, M. C.: A Bounds on the Resonant Frequency of Rectangular Microstrip Antennas. NASA TM-81882, 1980.

13. Bailey, M. C.; Croswell, William F.; and Kirby, Richard C.: Antennas and Wave Propagation. Electronics Engineers' Handbook, Donald G. Fink and Donald Christiansen, eds., McGraw-Hill, Inc., c.1982, pp. 18-1 - 18-126.

14. Sommerfeld, Arnold: Partial Differential Equations in Physics. Academic Press, Inc., 1949.

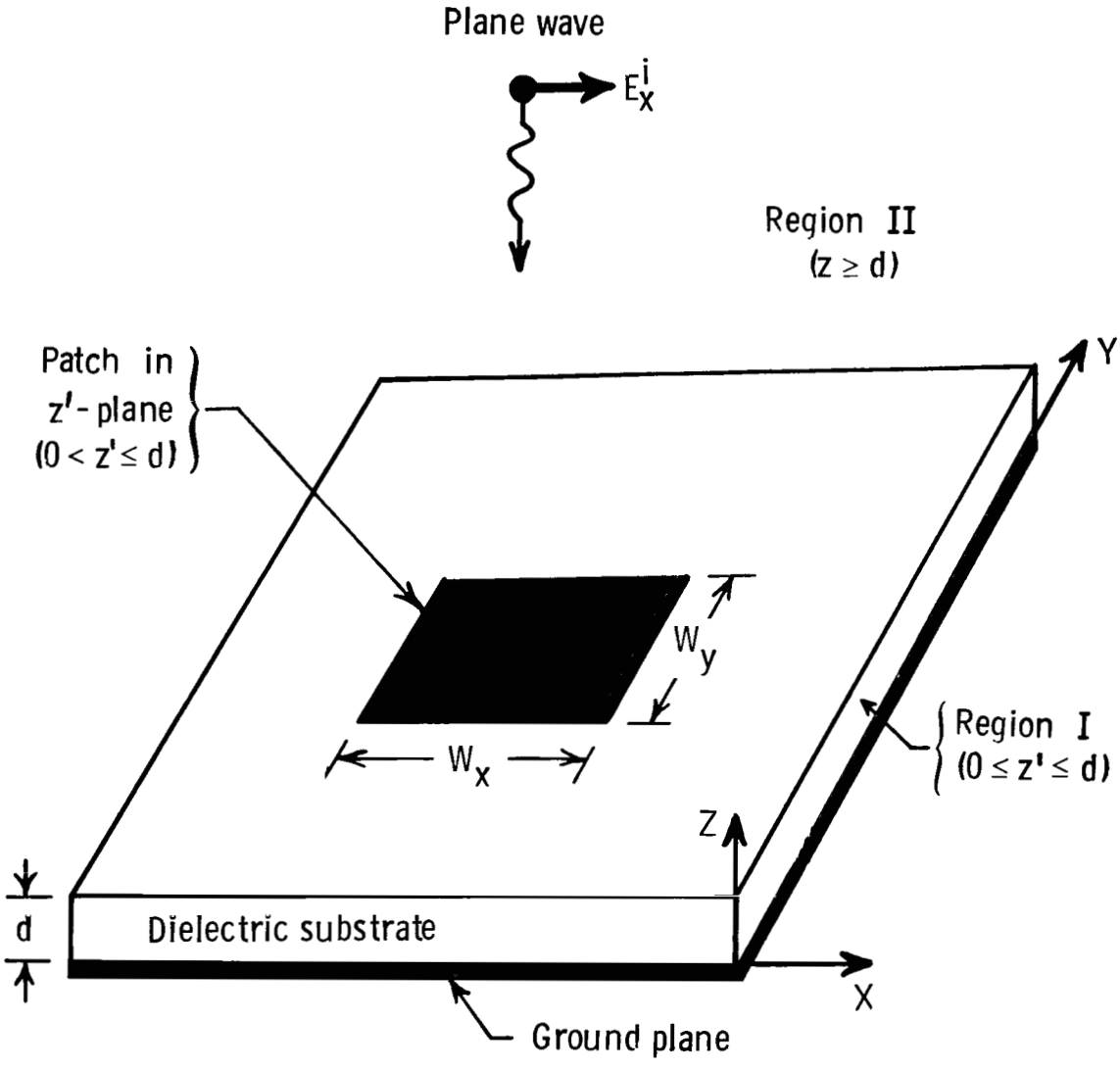

Figure 1.- Geometry of microstrip antenna.

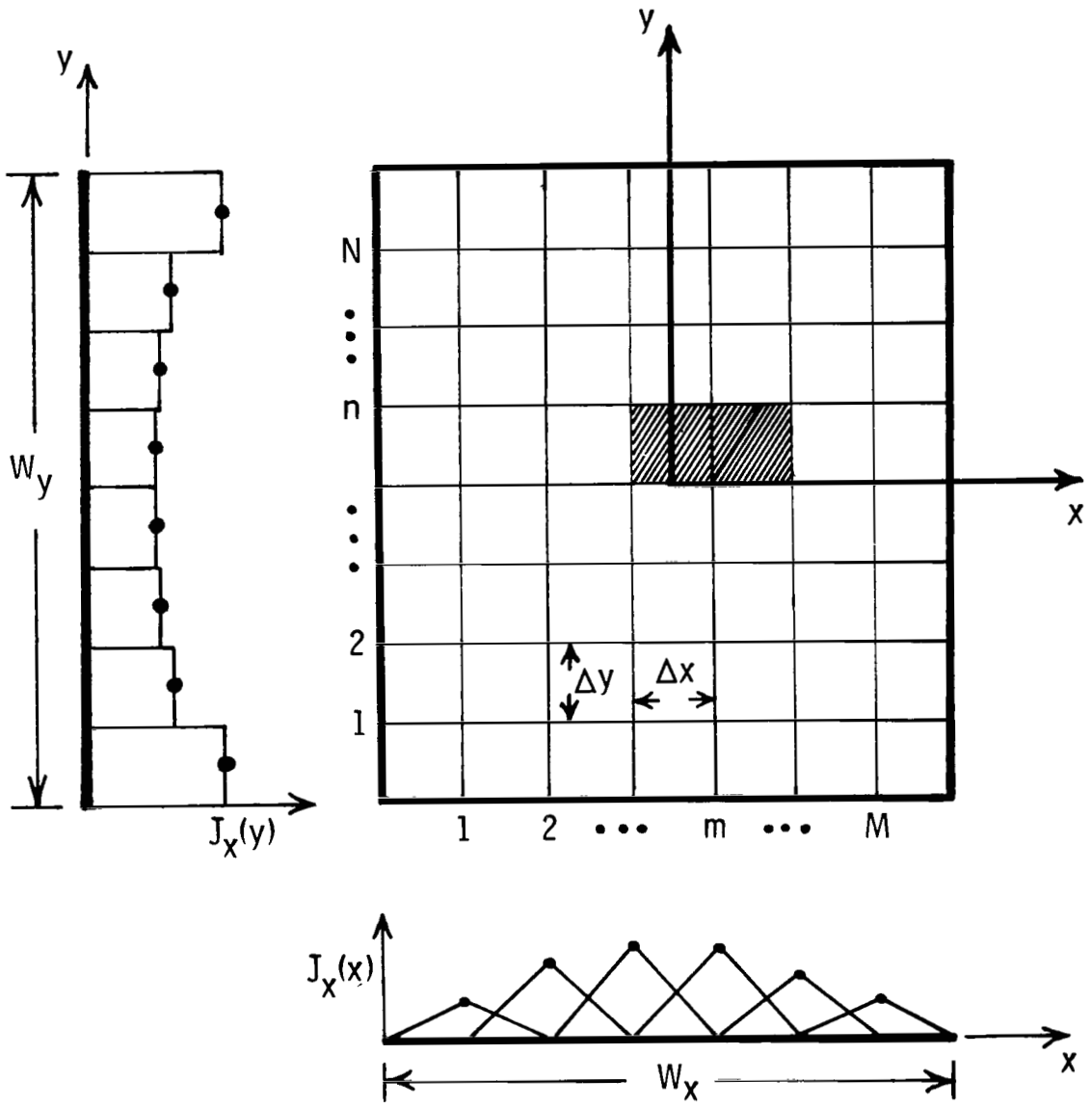

Figure 2.- Rectangular patch with pulse subdomains and x-directed current distribution.

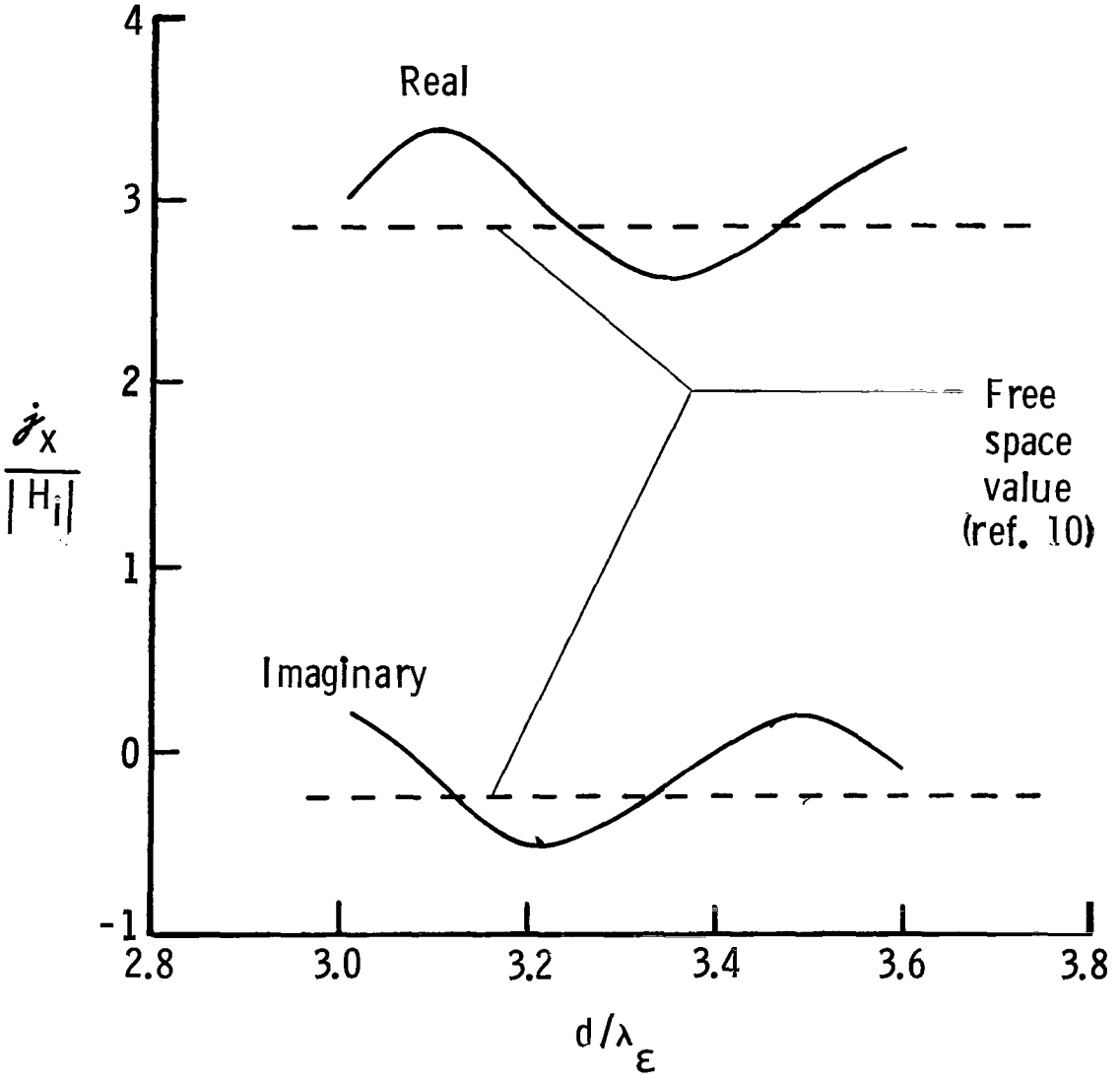

Figure 3.- Square patch current versus dielectric substrate thickness compared with free space value. $W_x = W_y = \lambda_\varepsilon$; $d = z'$; $\varepsilon_r = 1.0$.

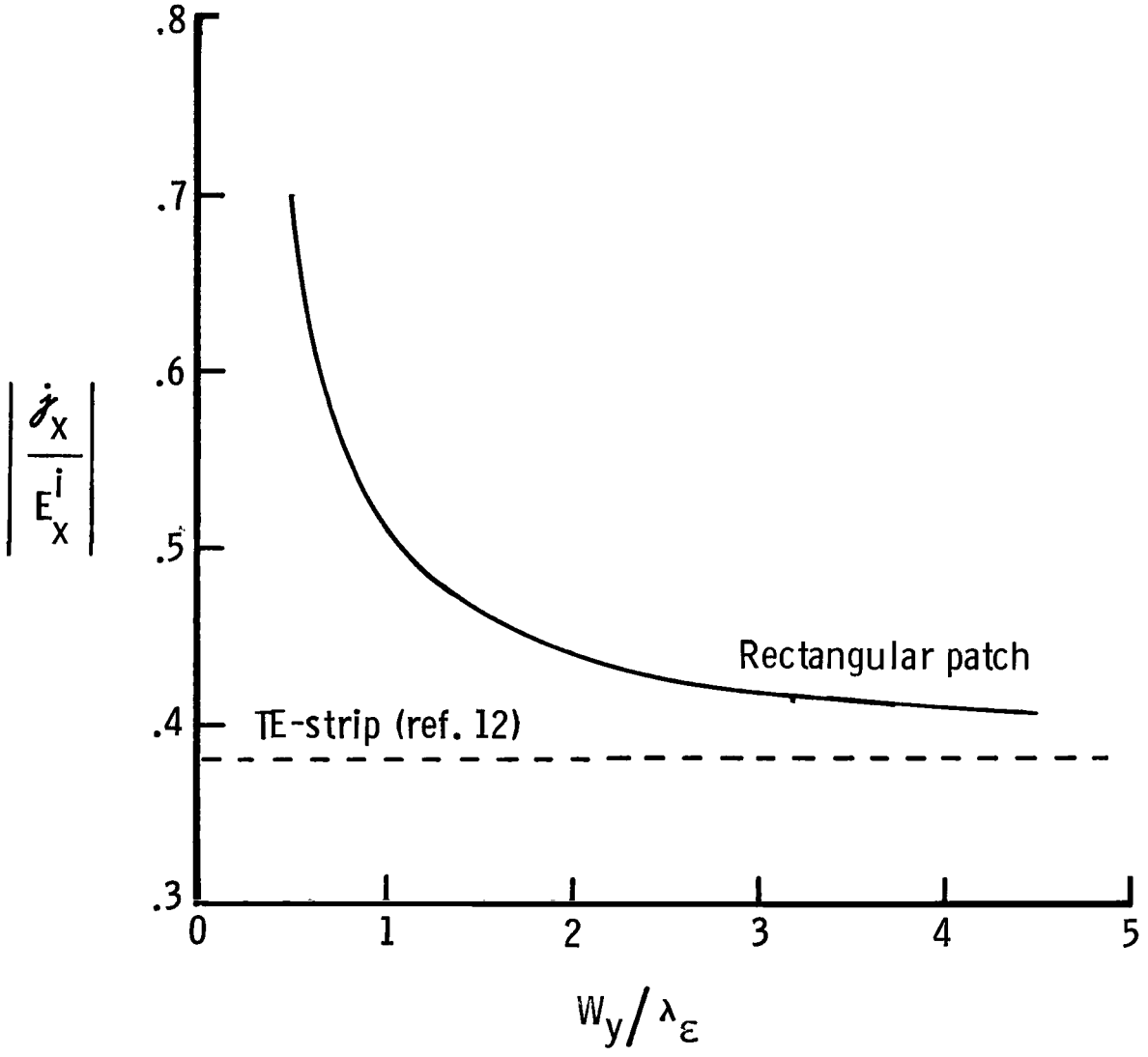

Figure 4.- Comparison of rectangular patch current with TE-strip current. $W_x = 0.5\lambda_\varepsilon$; $d = z' = 0.02\lambda_\varepsilon$; $\varepsilon_r = 2.5$.

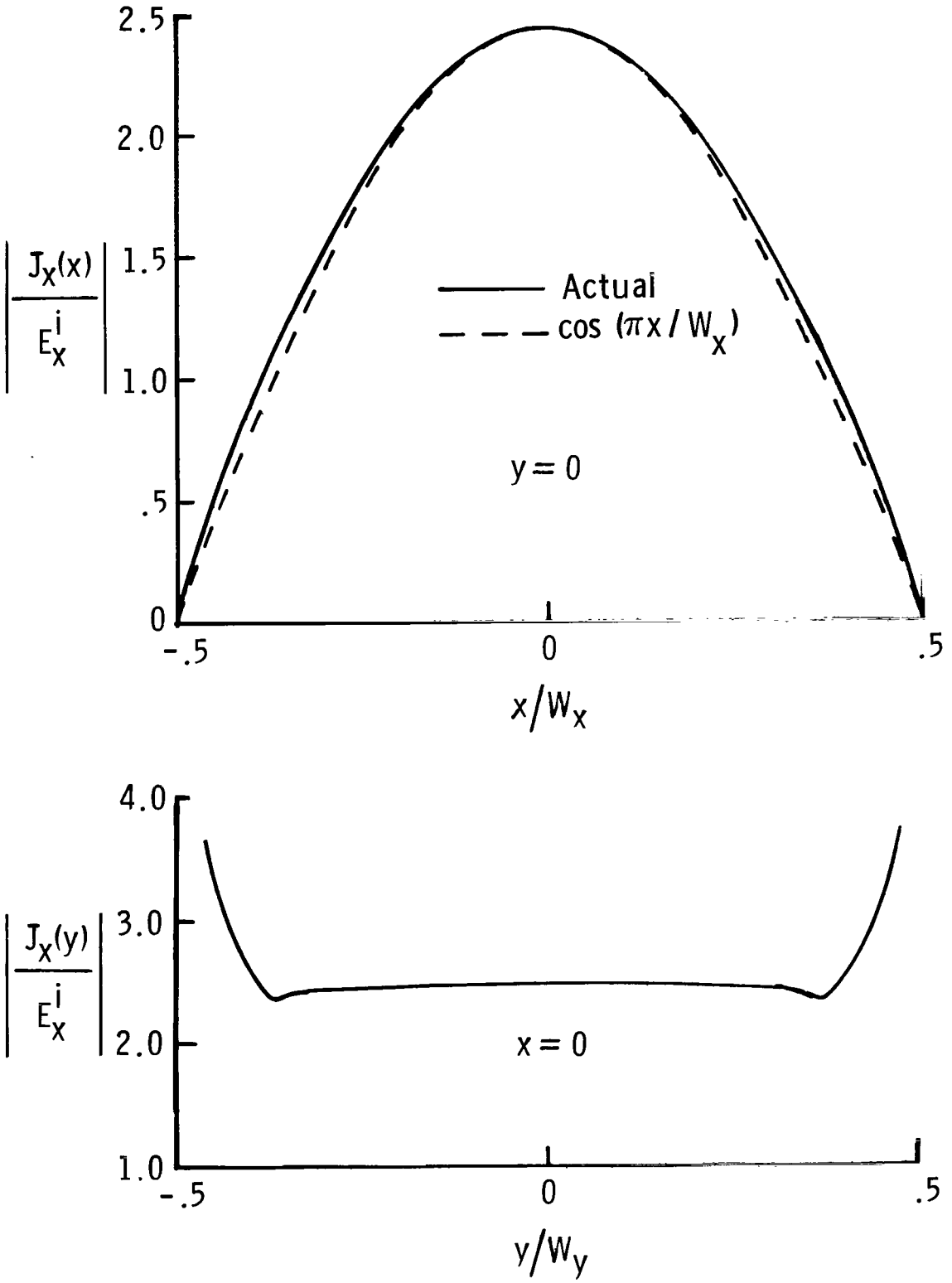

Figure 5.- Patch current distribution for a square patch. $W_x = W_y = 0.485\lambda_\varepsilon$; $d = z' = 0.02\lambda_\varepsilon$; $\varepsilon_r = 2.5$.

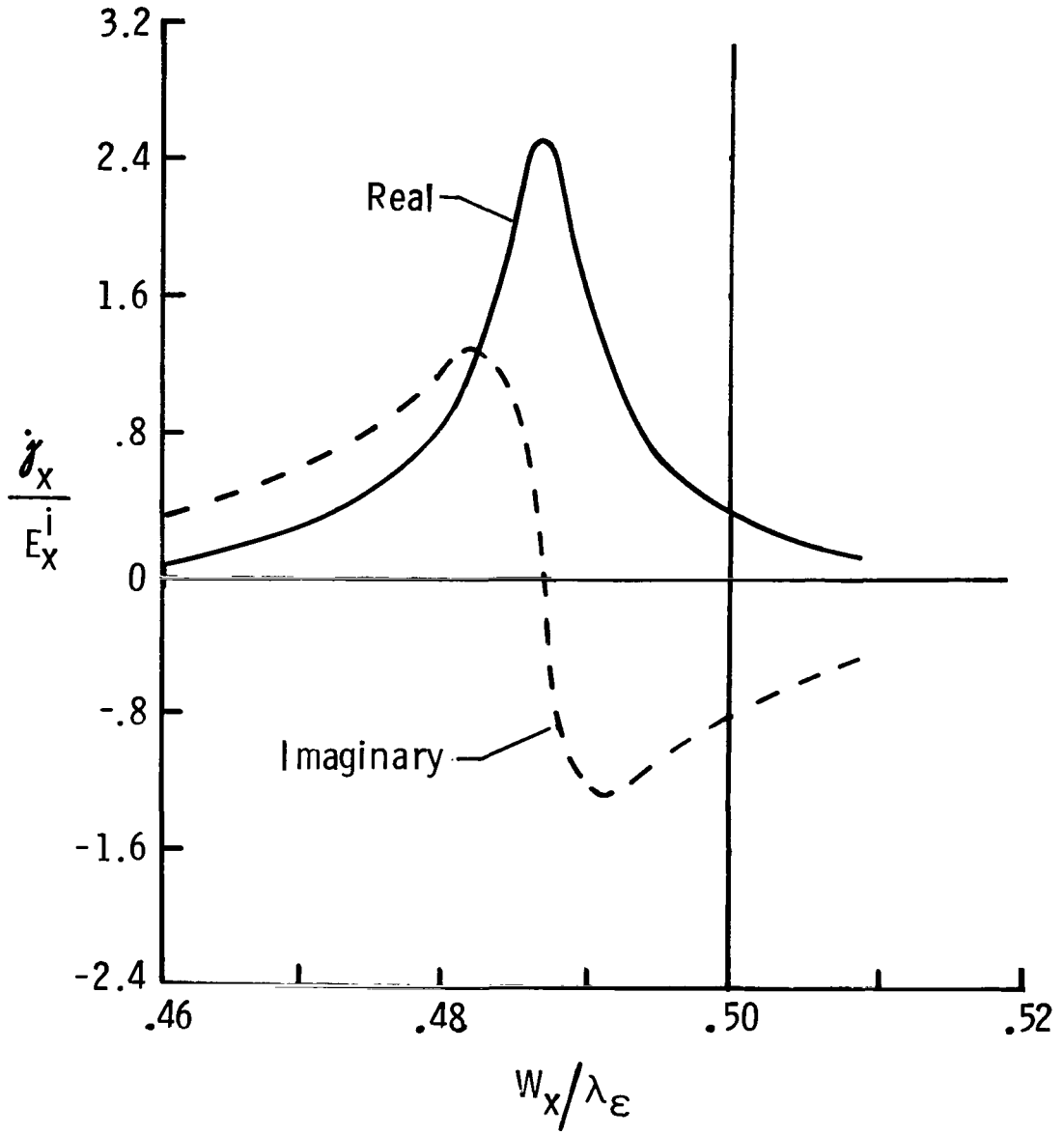

Figure 6.- Complex current coefficient versus dimension of square patch. $W_x = W_y$; $d = z' = 0.02\lambda_\varepsilon$; $\varepsilon_r = 2.5$.

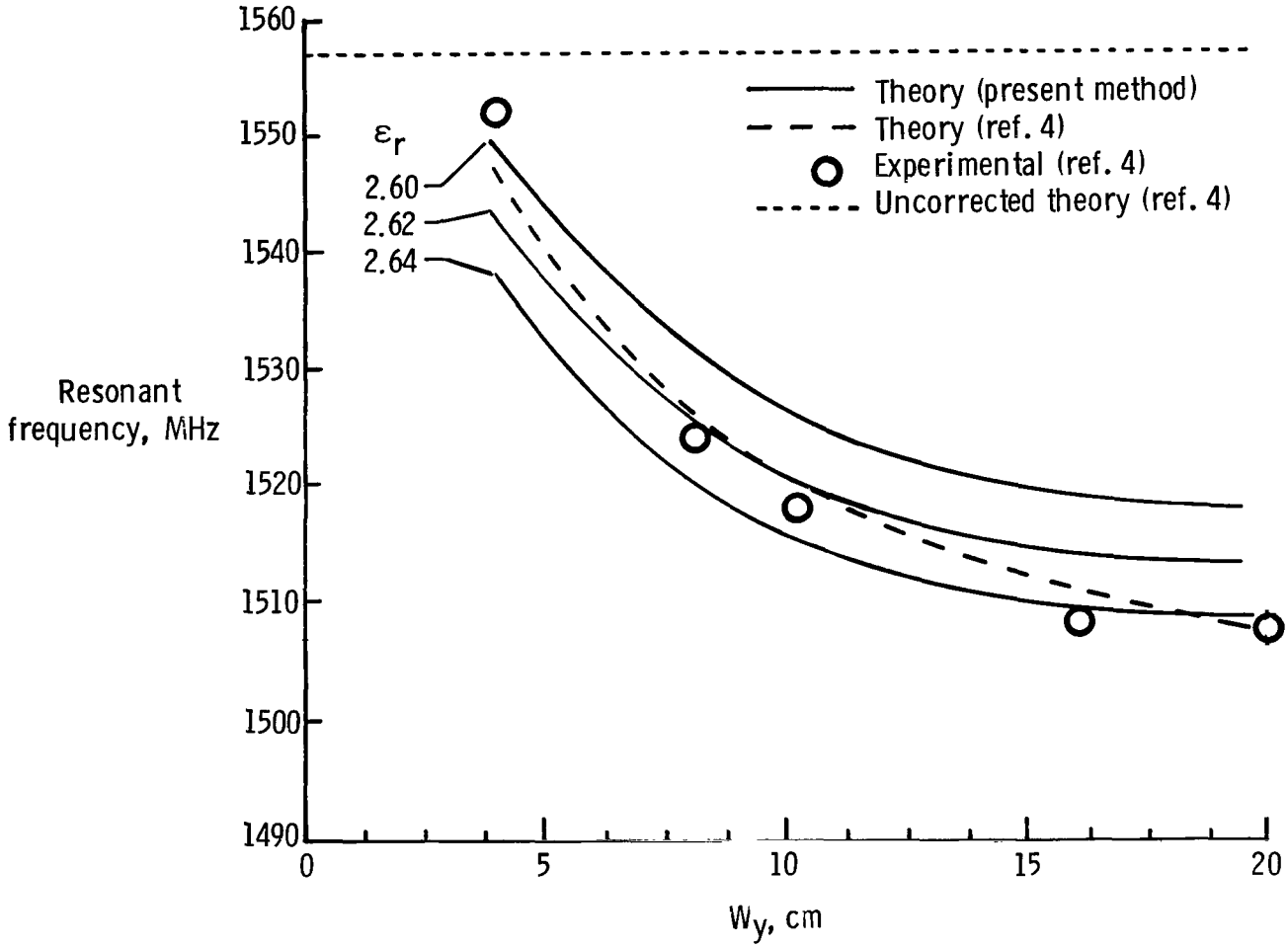

Figure 7.- Resonant frequency of rectangular patch versus H-plane dimension. W_x = 5.95 cm; d = z' = 0.159 cm; ε_r = 2.62 ± 0.02 .

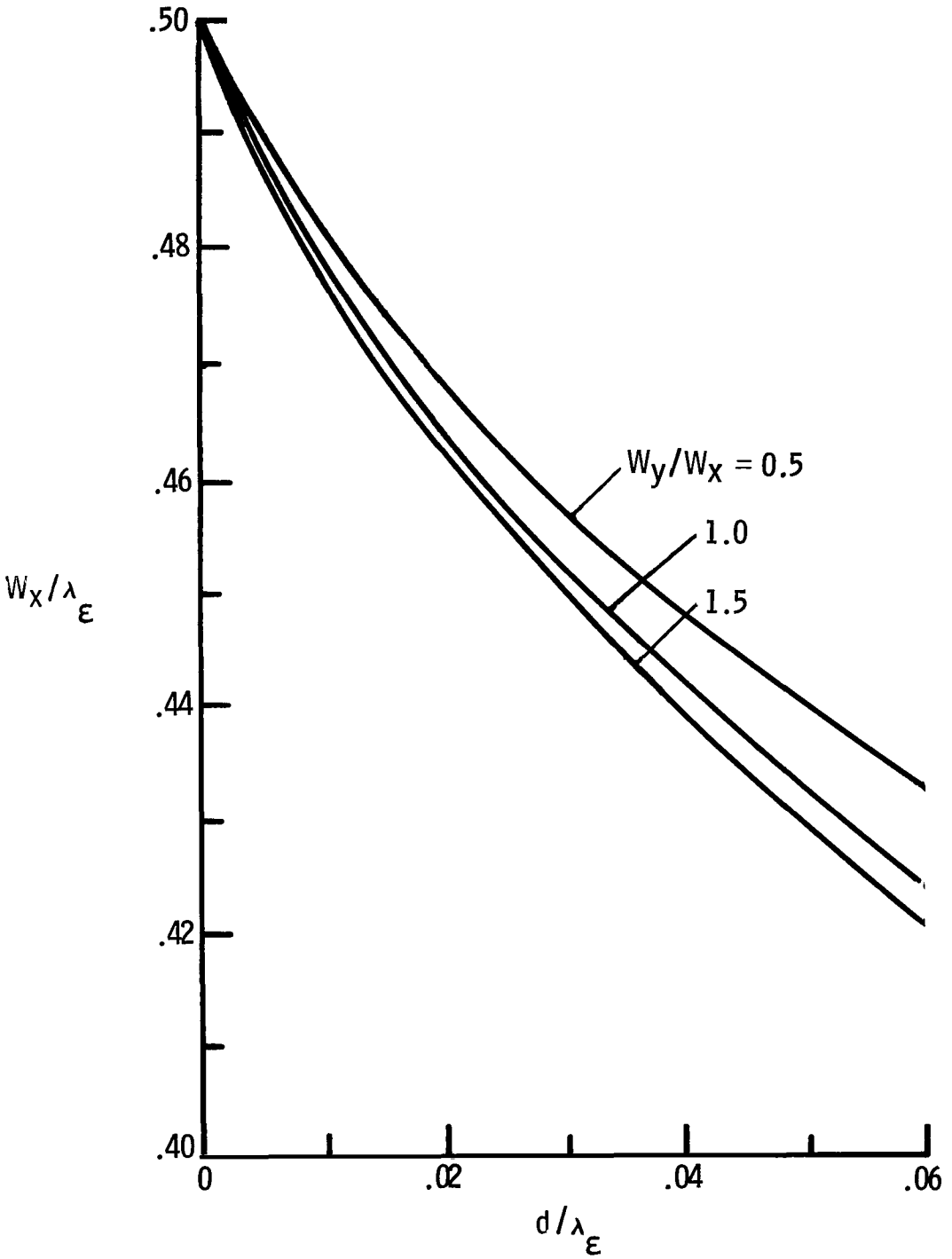

Figure 8.- Resonant width of rectangular patch versus substrate thickness for $z' = d$ and $\varepsilon_r = 1.0$.

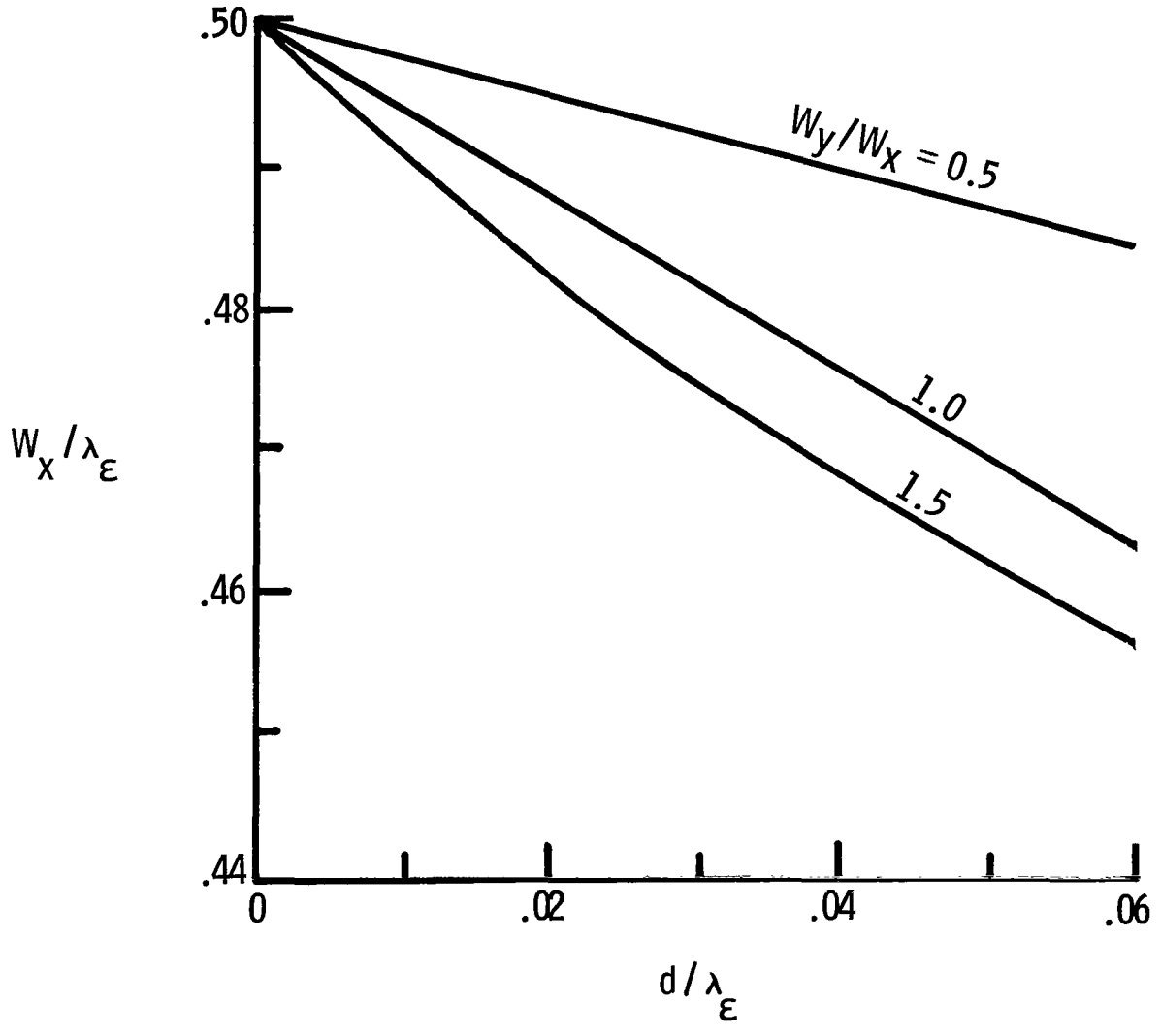

Figure 9.- Resonant width of rectangular patch versus substrate thickness for $z' = d$ and $\varepsilon_r = 2.5$.

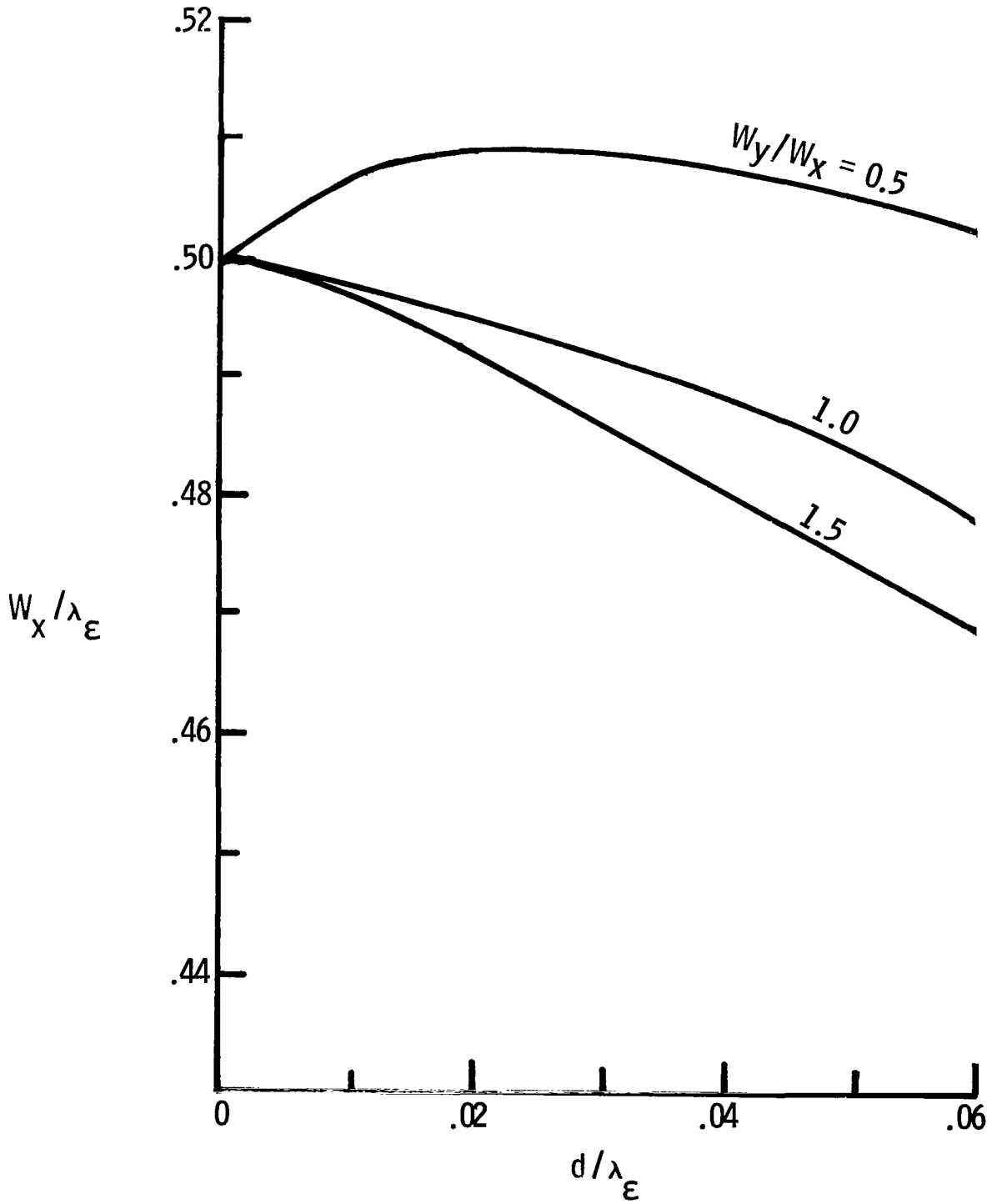

Figure 10.- Resonant width of rectangular patch versus substrate thickness for $z' = d$ and $\varepsilon_r = 6.0$.

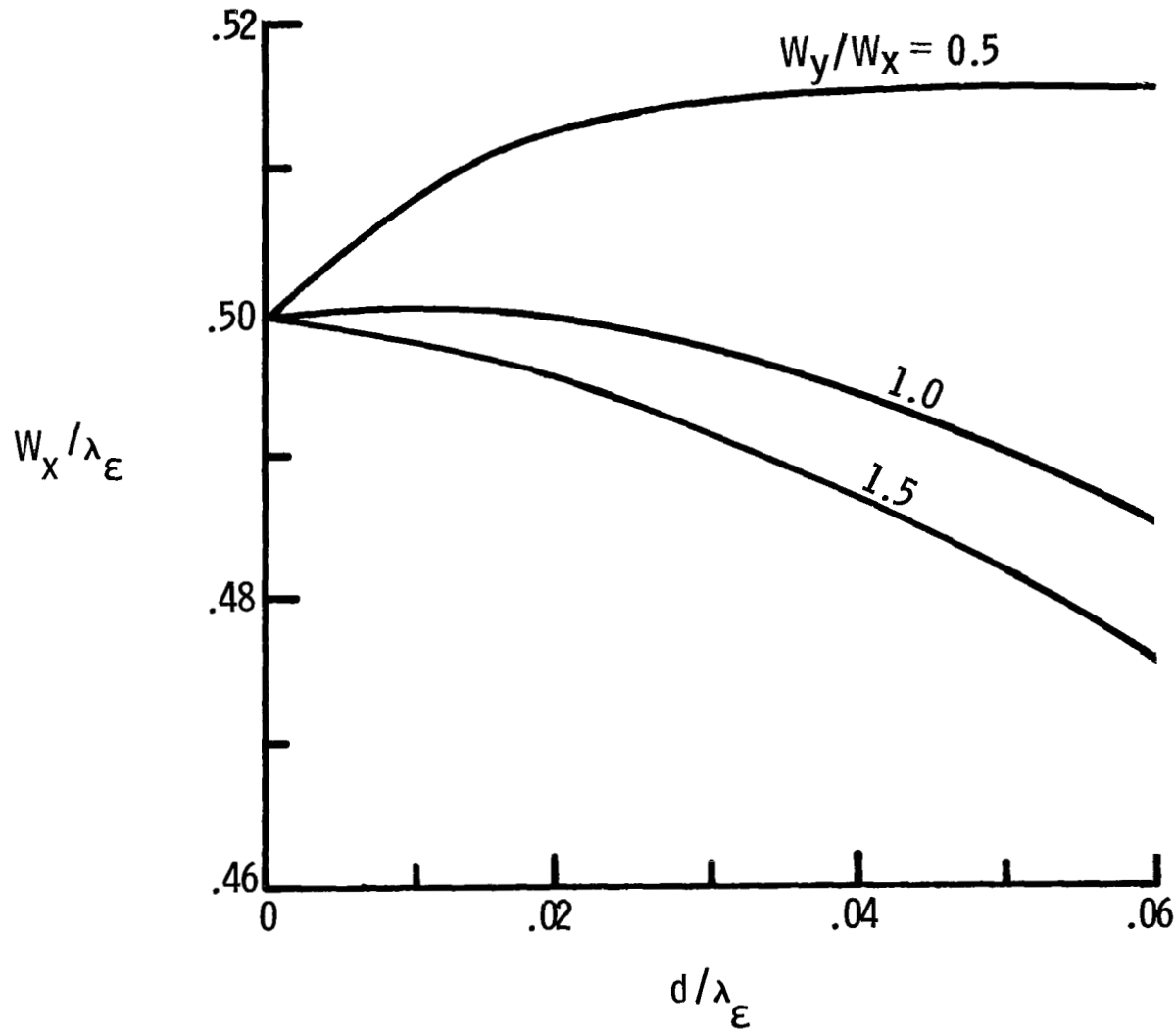

Figure 11.- Resonant width of rectangular patch versus substrate thickness for $z' = d$ and $\varepsilon_r = 10.0$.

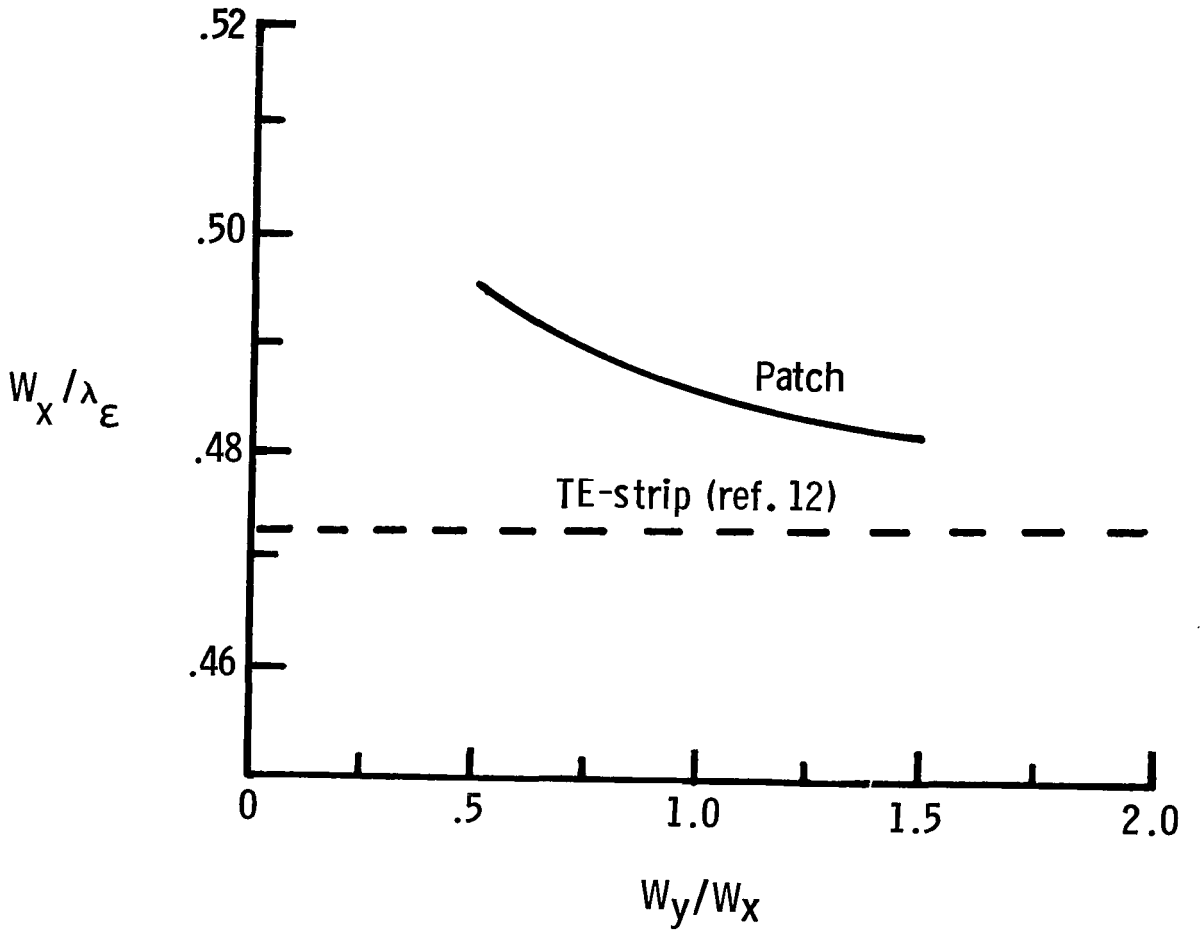

Figure 12.- Resonant width of rectangular patch versus aspect ratio compared with resonant width of strip for $z' = d = 0.02\lambda_\varepsilon$ and $\varepsilon_r = 2.5$.

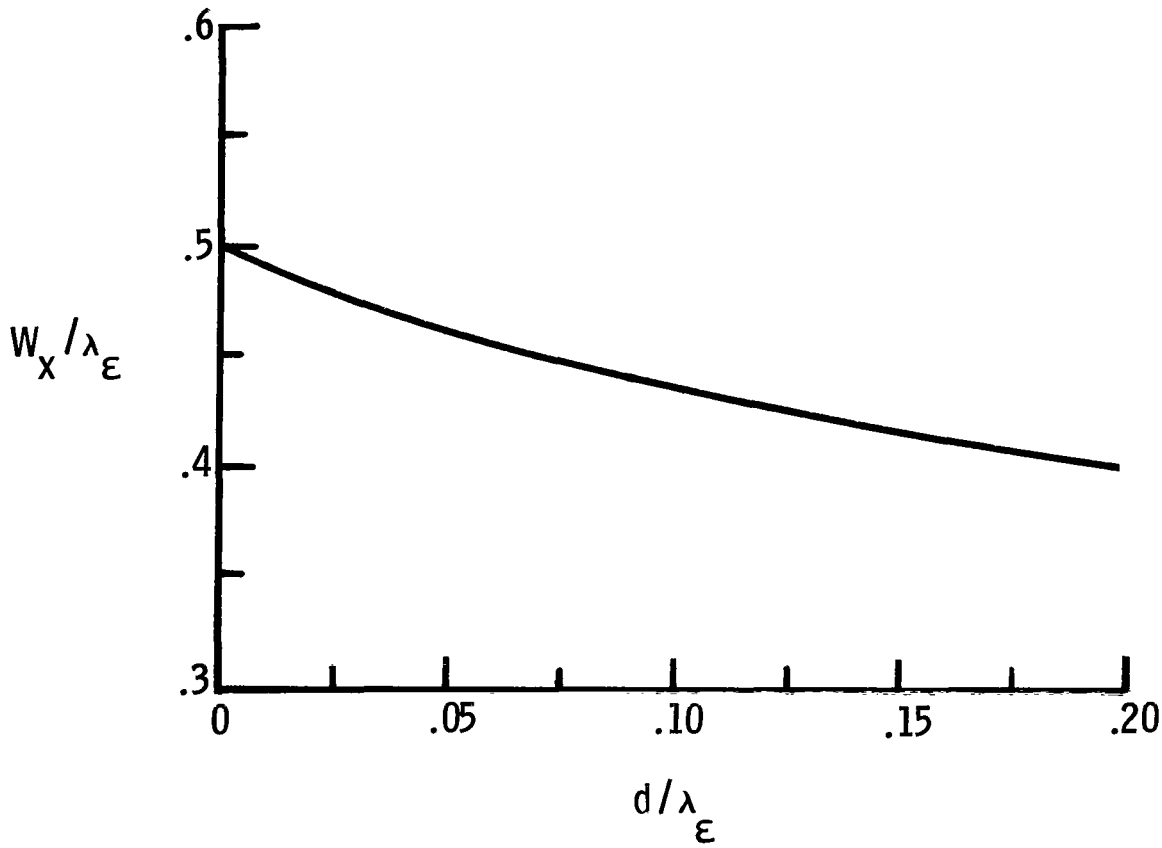

Figure 13.- Resonant width of square patch for thick substrates.
$z' = d$; $\varepsilon_r = 2.5$.

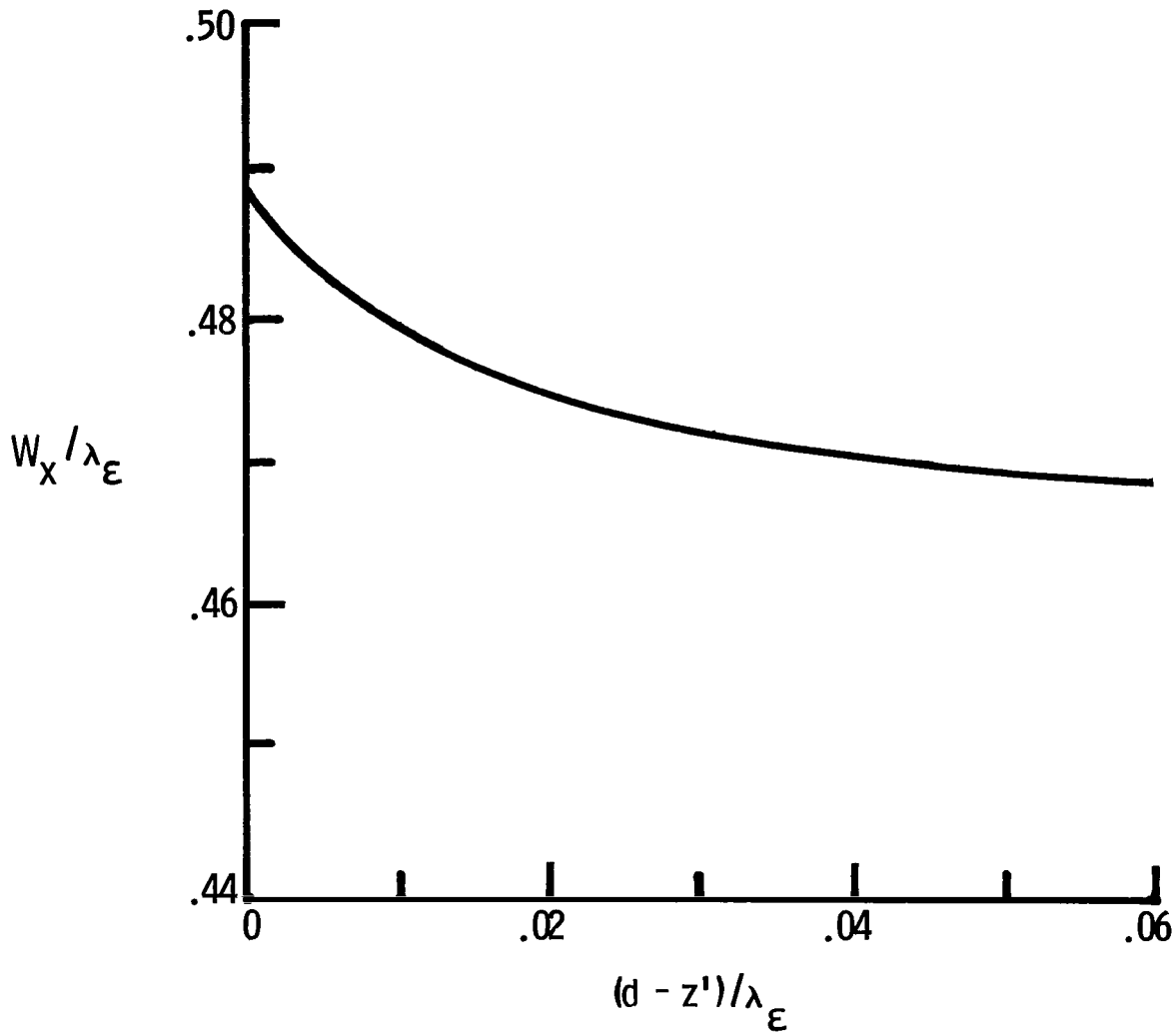

Figure 14.- Resonant width of dielectric-coated square patch versus coating thickness. $z' = 0.0175\lambda_\varepsilon$; $\varepsilon_r = 2.5$.

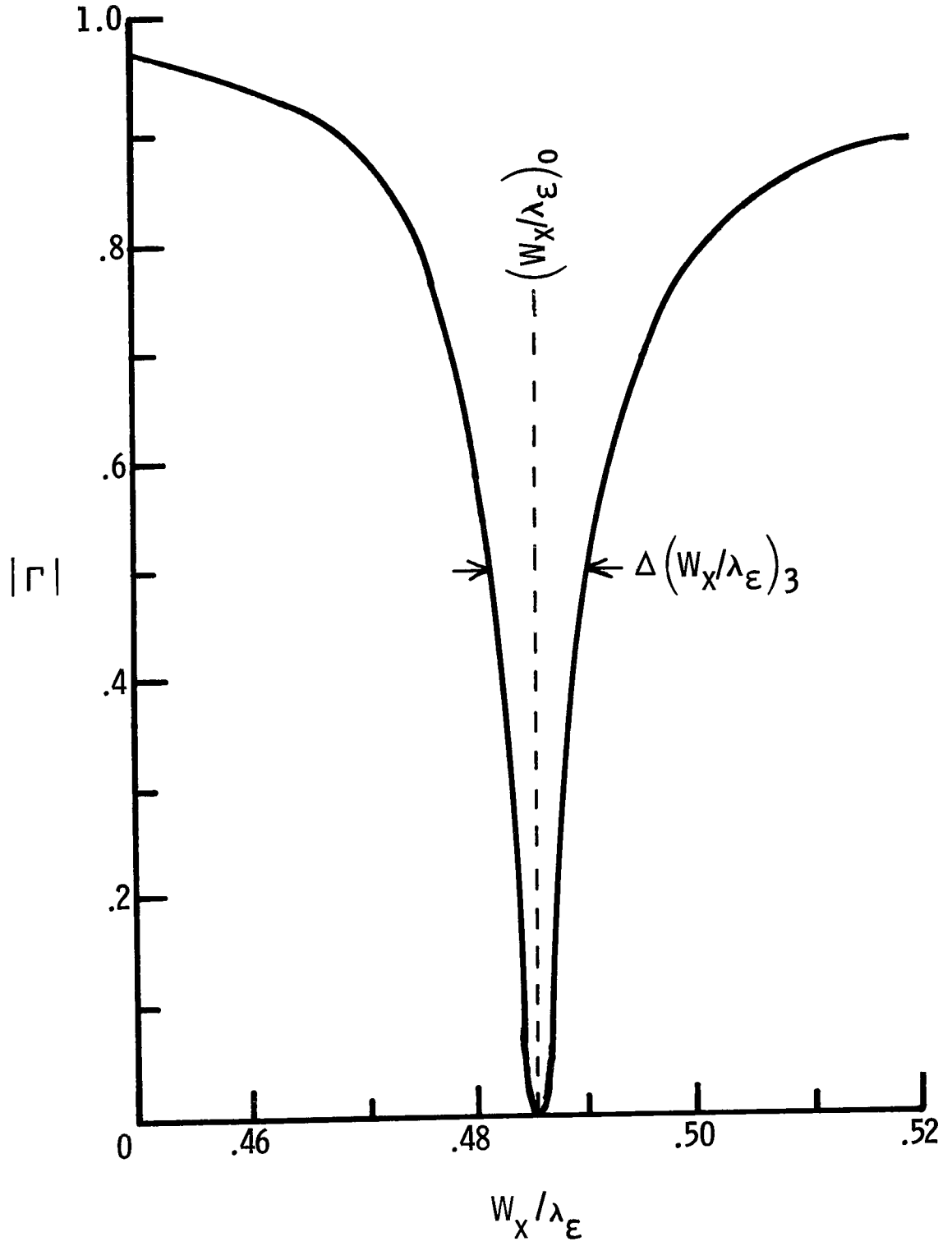

Figure 15.- Input reflection coefficient versus patch size for square patch. $z' = d = 0.02\lambda_\varepsilon$; $\varepsilon_r = 2.5$.

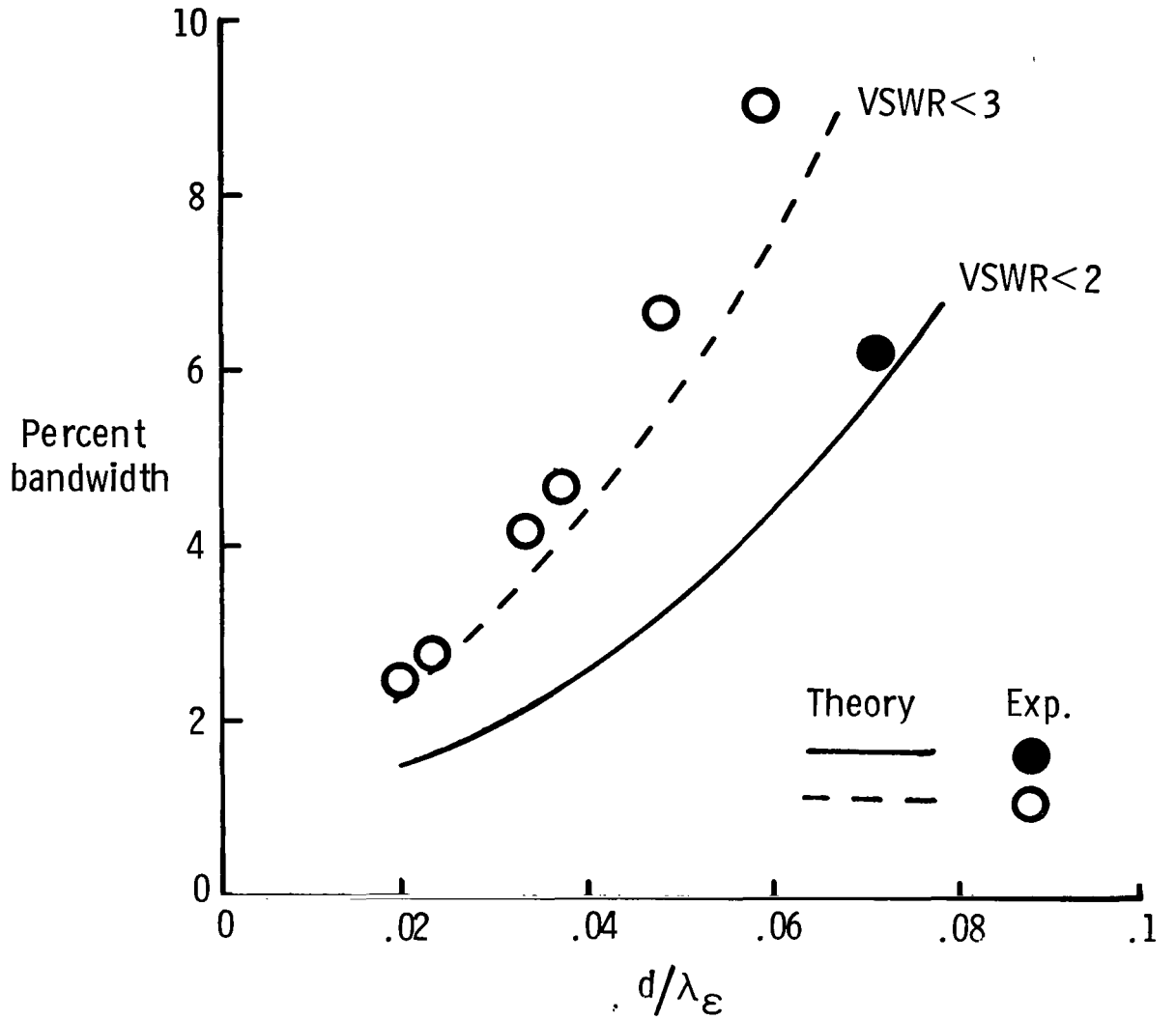

Figure 16.- Comparison of measured with calculated bandwidths for square microstrip antenna. $z' = d$; $\varepsilon_r = 2.5$.

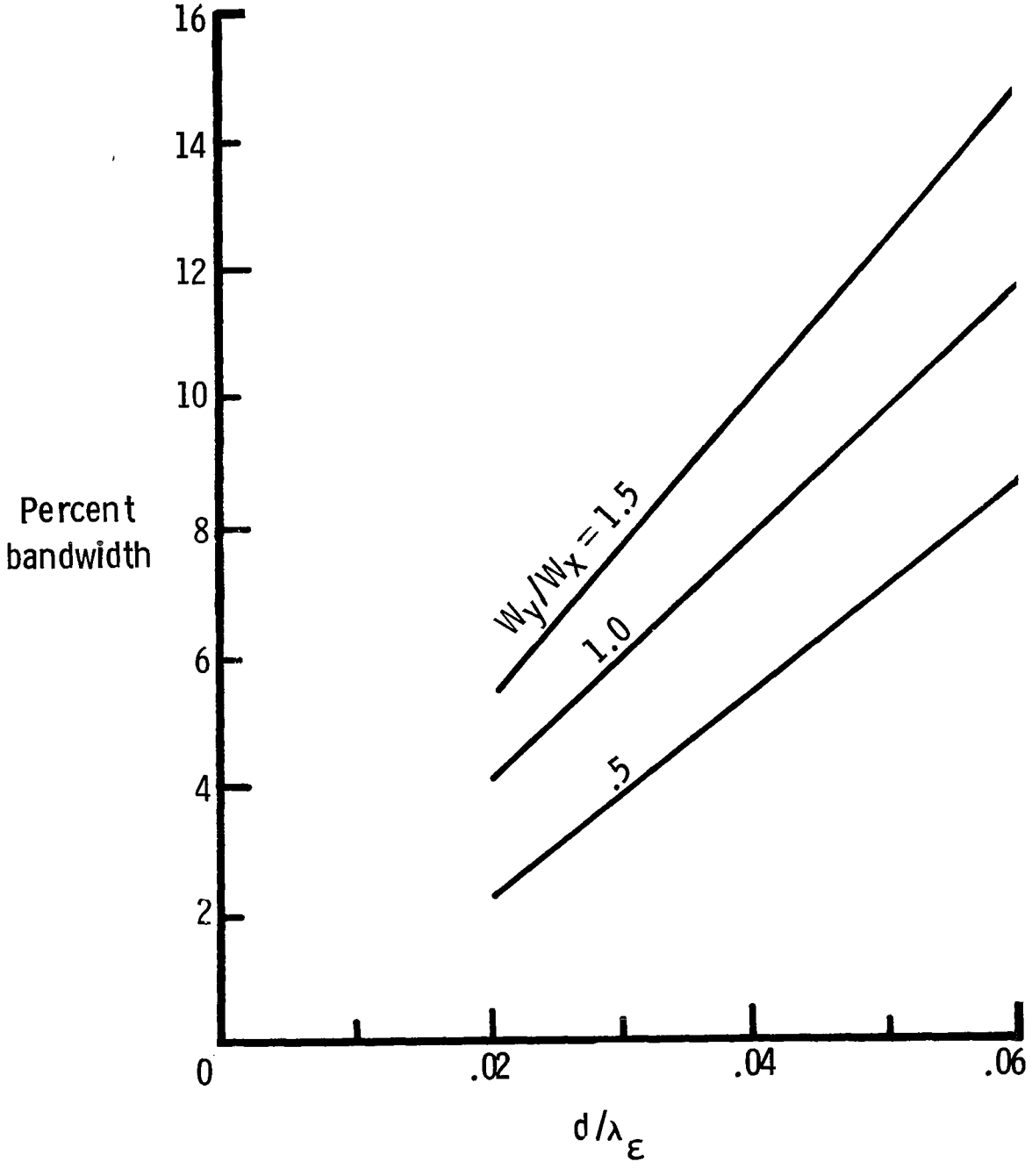

Figure 17.- Calculated percent bandwidth for rectangular patch for $\varepsilon_r = 1.0$. VSWR < 3; z' = d.

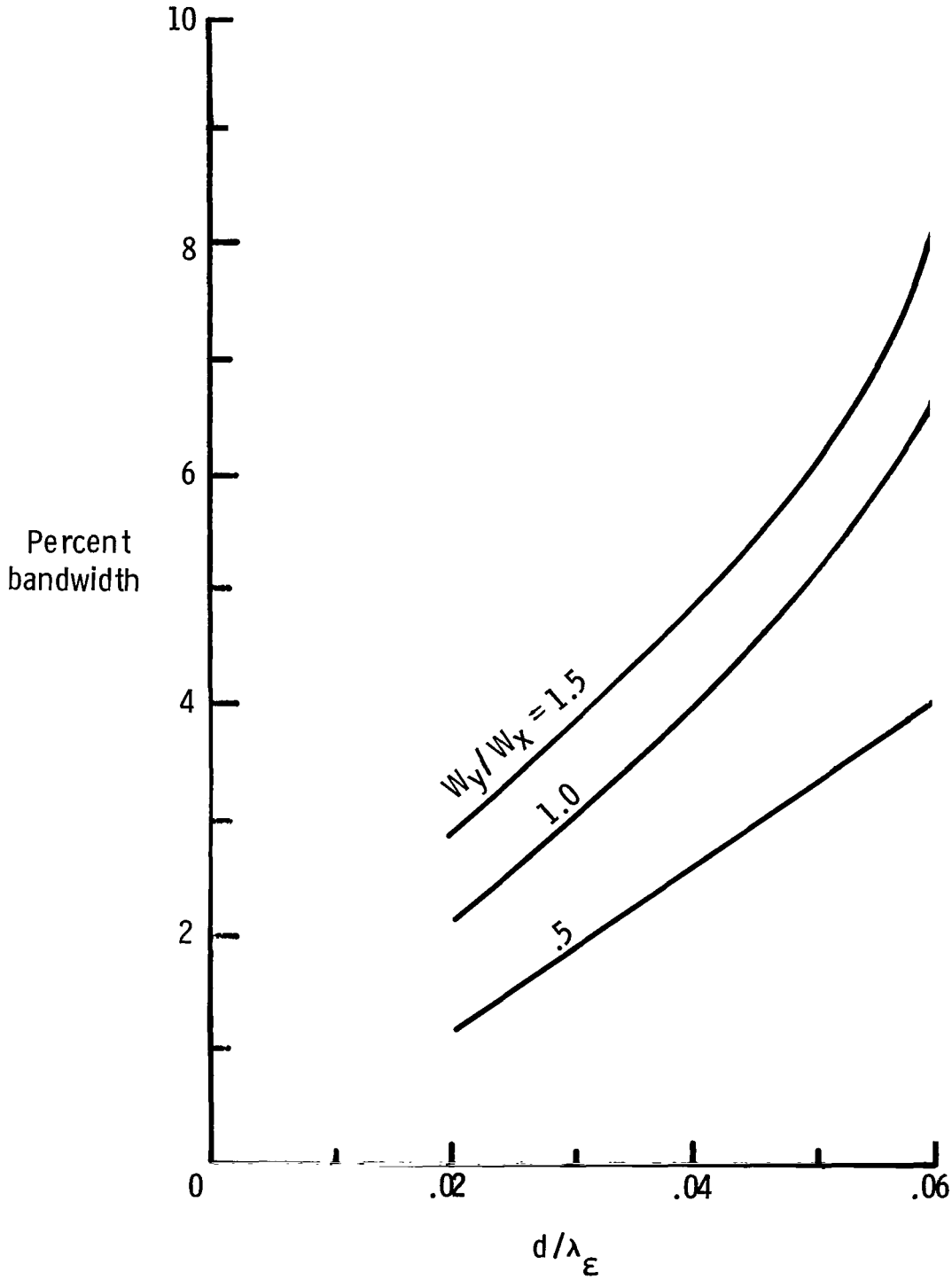

Figure 18.- Calculated percent bandwidth for rectangular patch for $\varepsilon_r = 2.5$. VSWR < 3; z' = d.

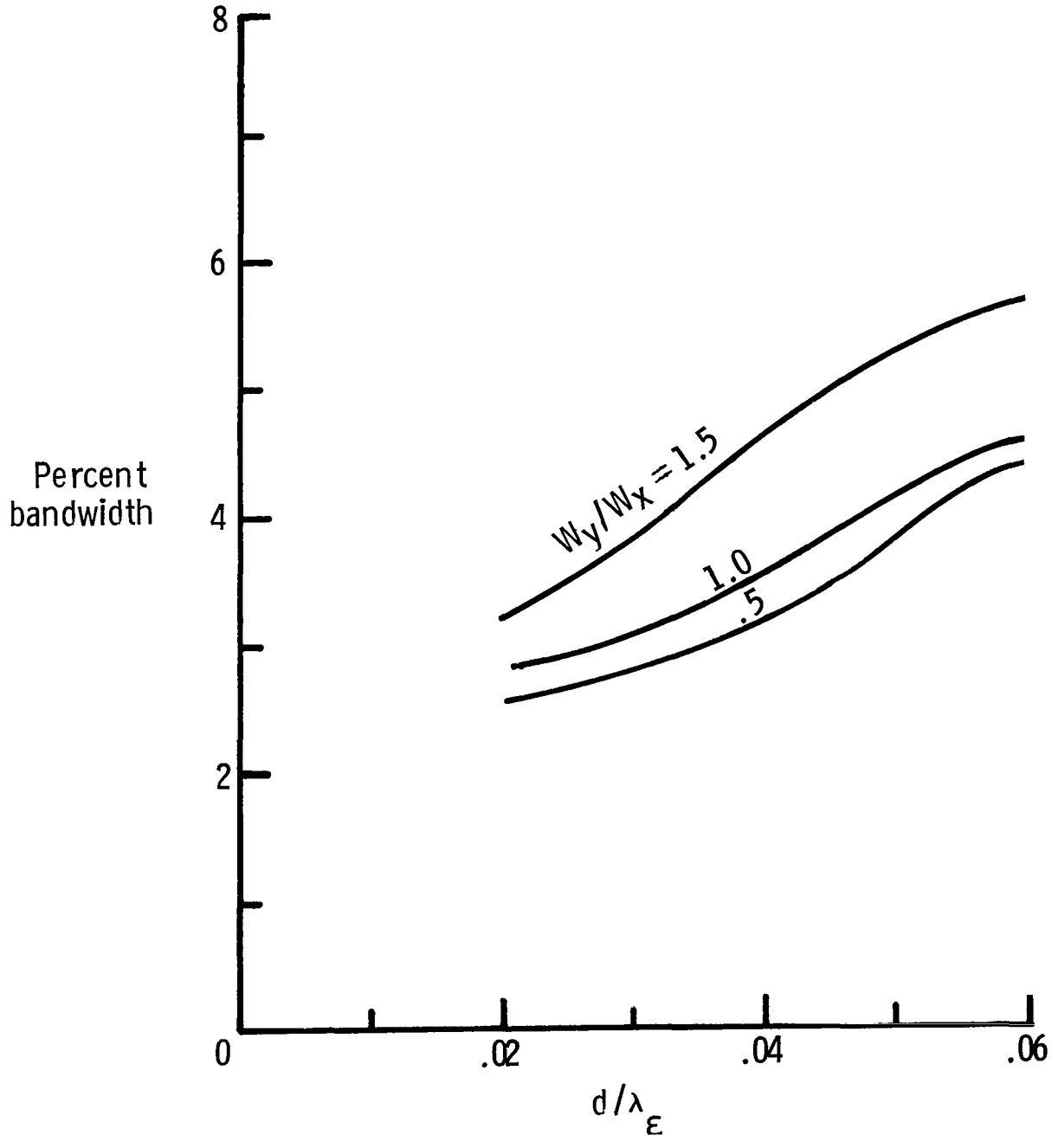

Figure 19.- Calculated percent bandwidth for rectangular patch for $\varepsilon_r = 6.0$. VSWR < 3; z' = d.

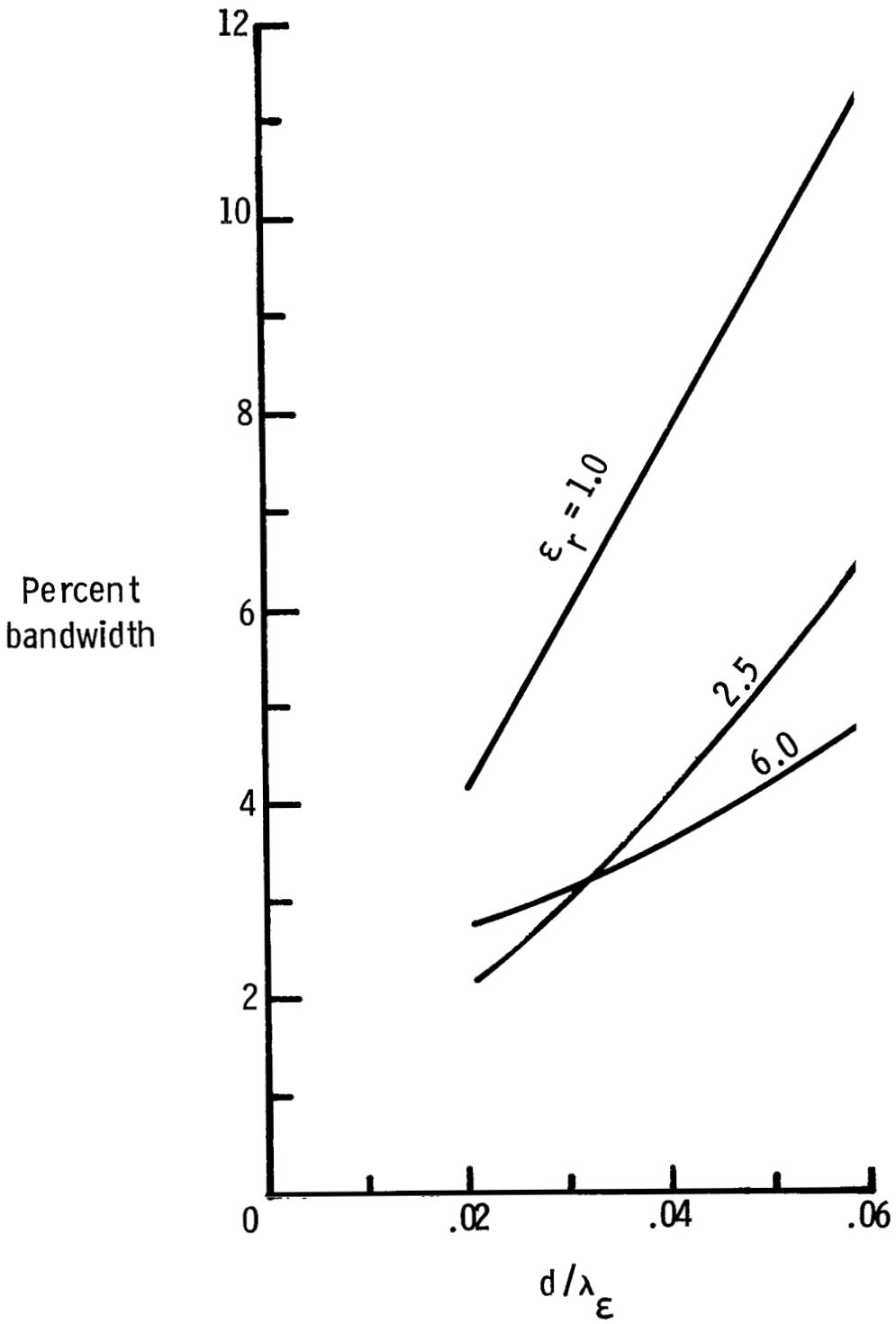

Figure 20.- Calculated percent bandwidth for square patch for VSWR < 3. z' = d.

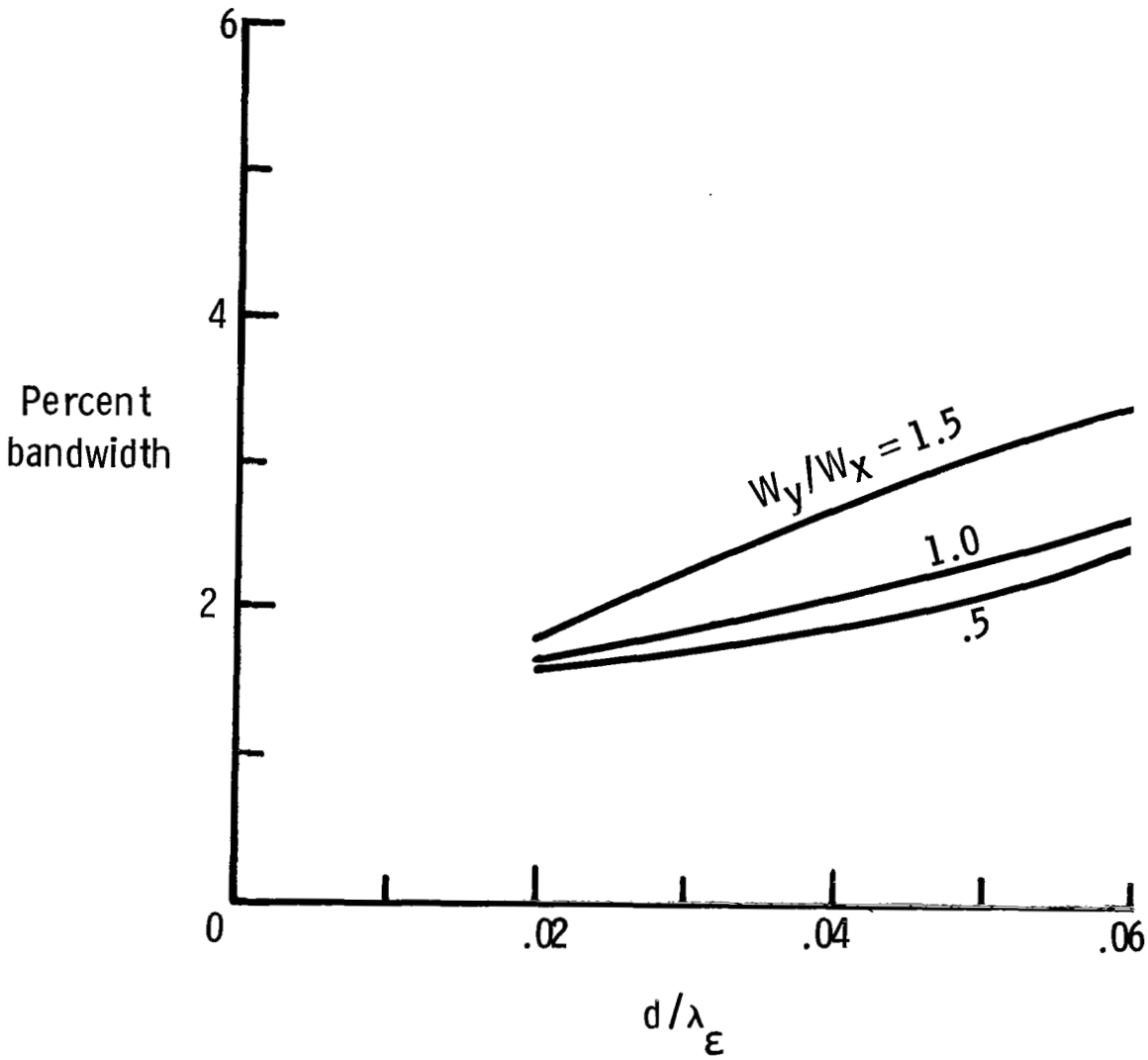

Figure 21.- Calculated percent bandwidth for rectangular patch for $\varepsilon_r = 6.0$. VSWR < 2; z' = d.

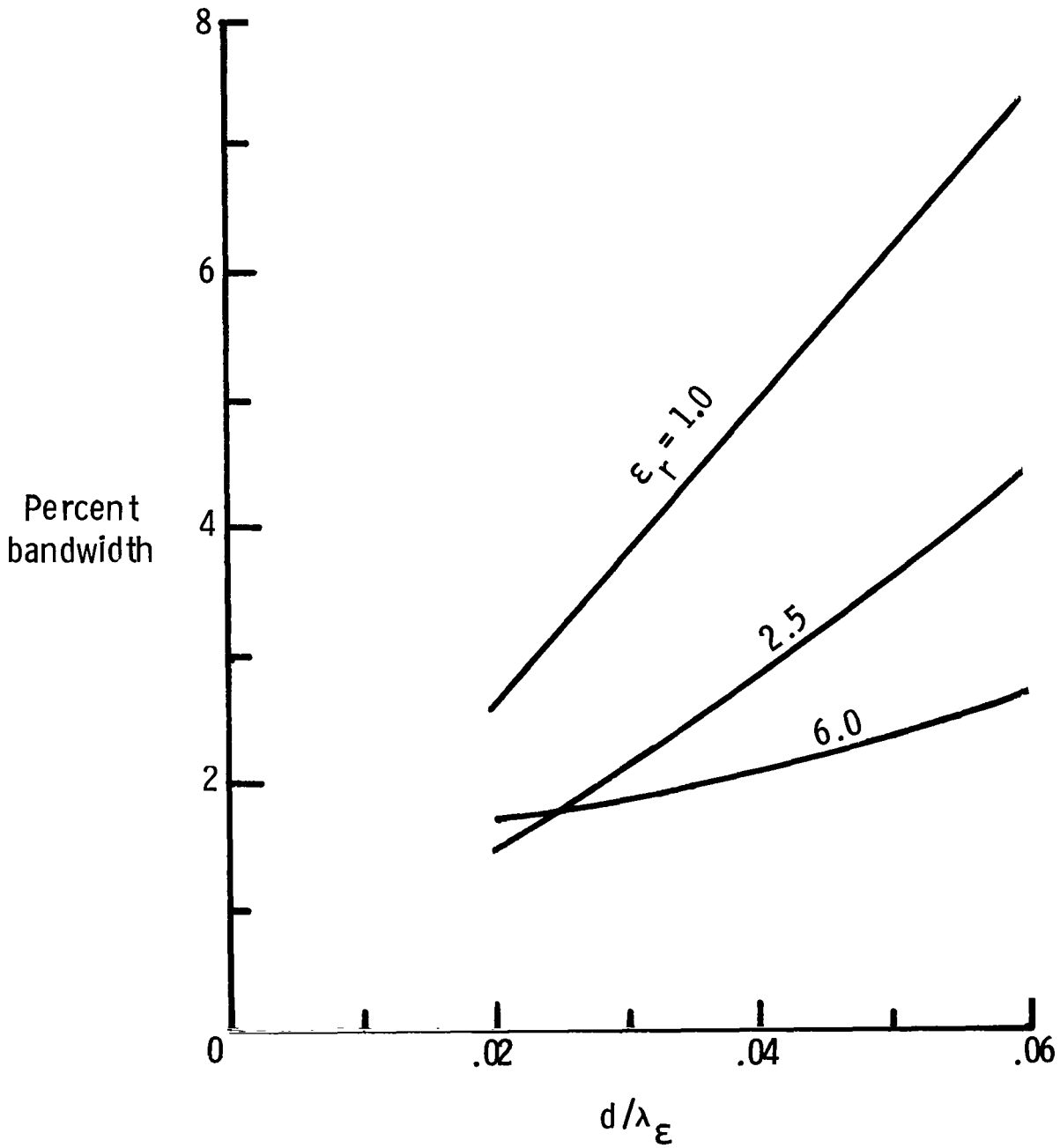

Figure 22.- Calculated percent bandwidth for square patch for VSWR < 2. z' = d.

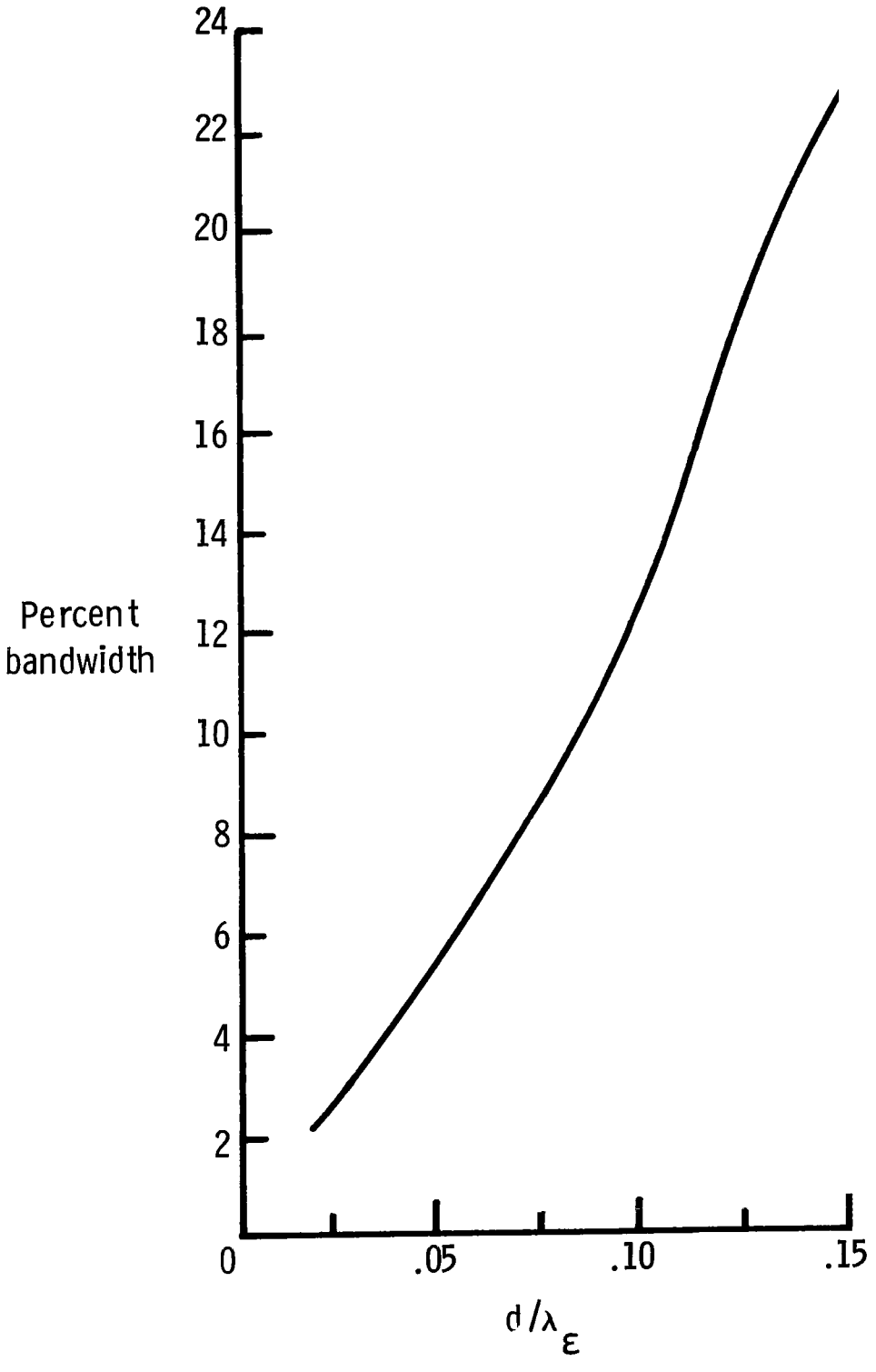

Figure 23.- Calculated percent bandwidth for square patch with thick dielectric substrate for VSWR < 3. $z' = d$; $\varepsilon_r = 2.5$.

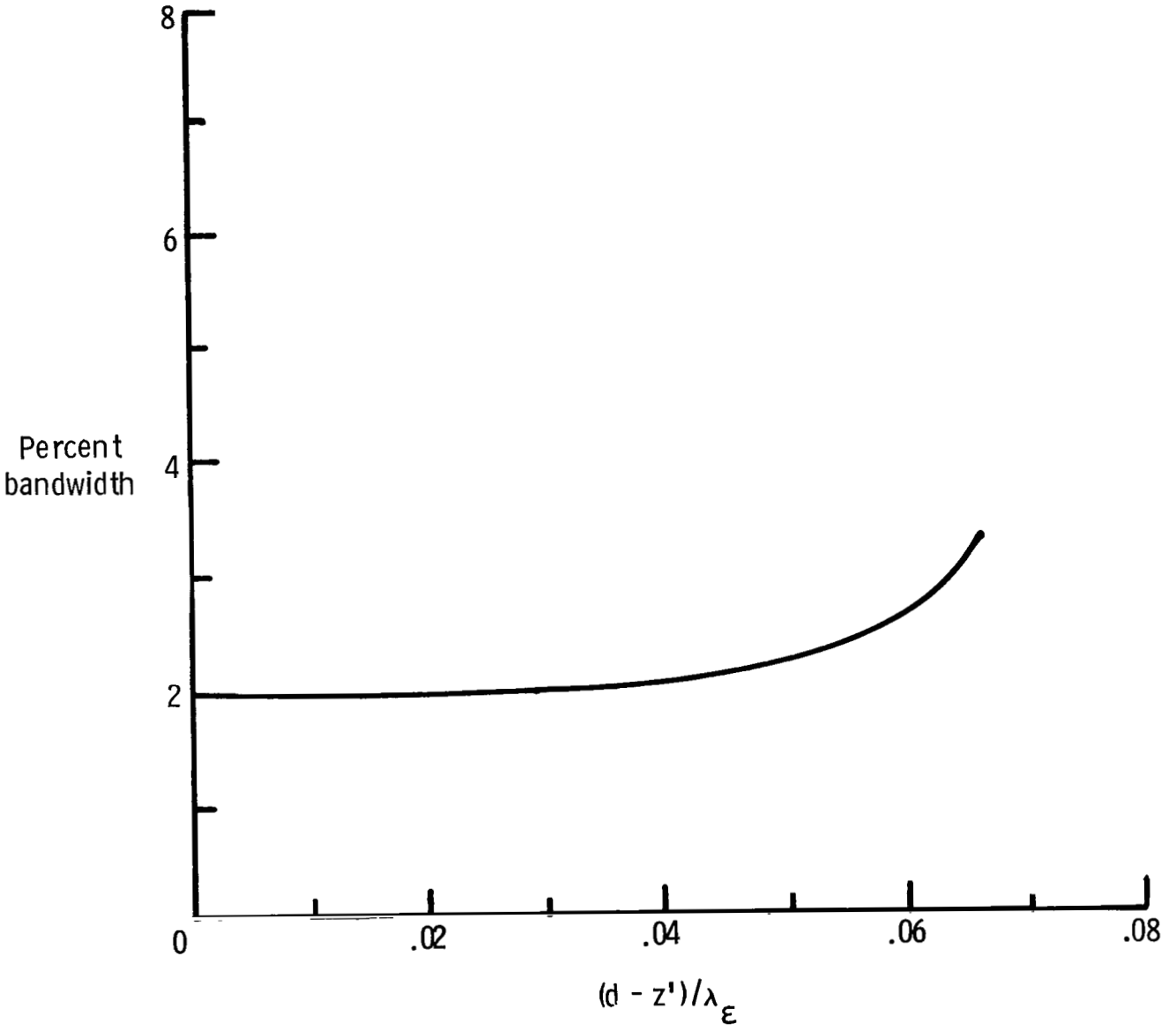

Figure 24.- Calculated percent bandwidth for dielectric-coated square patch for VSWR < 3. $z' = 0.0175\lambda_\varepsilon$; $\varepsilon_r = 2.5$.

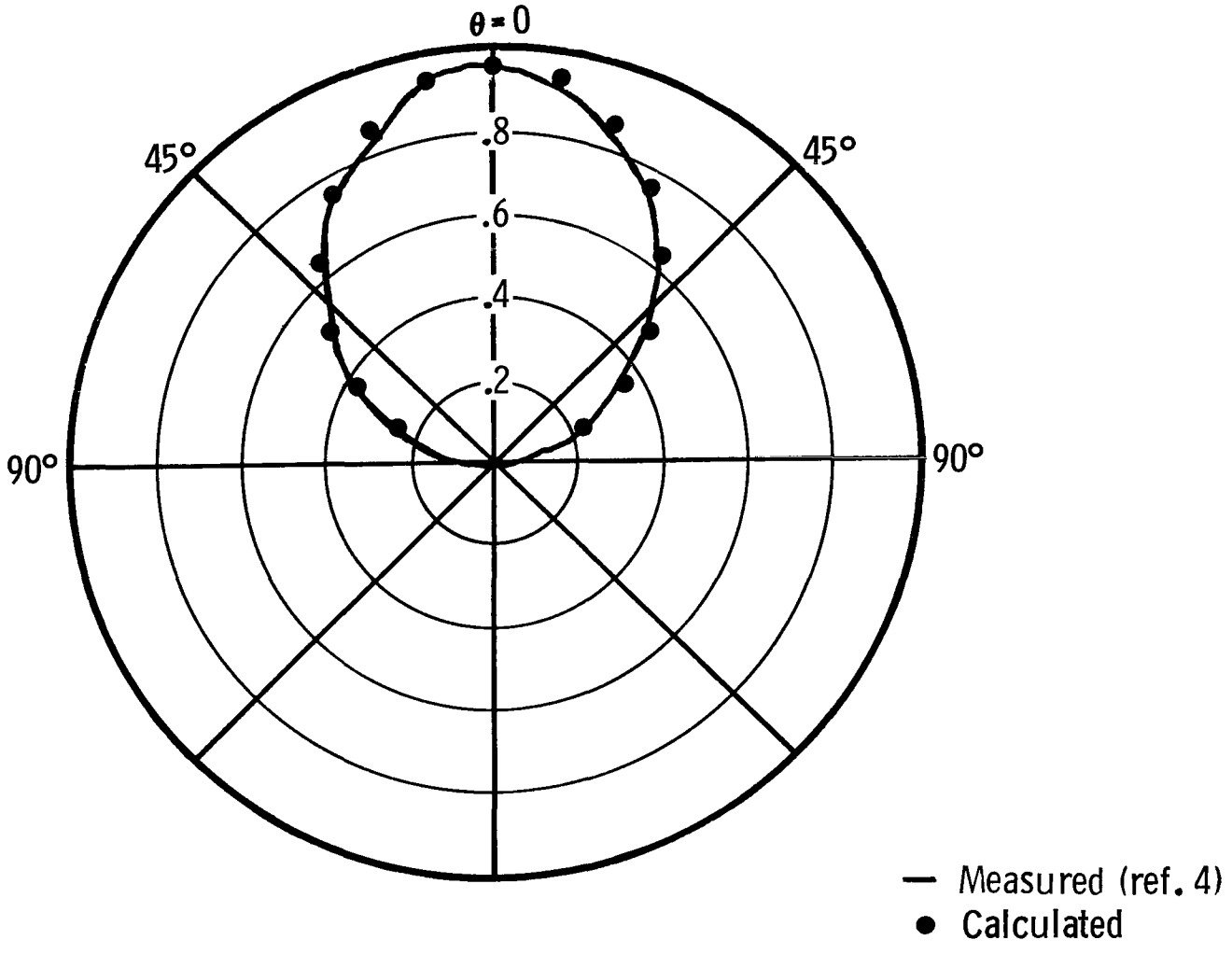

(a) H-plane pattern. $\phi = \pi/2$.

Figure 25.- Radiation pattern for 1187-MHz rectangular-patch antenna. W_x = 7.6 cm; W_y = 11.43 cm; z' = d = 0.158 cm; ε_r = 2.62.

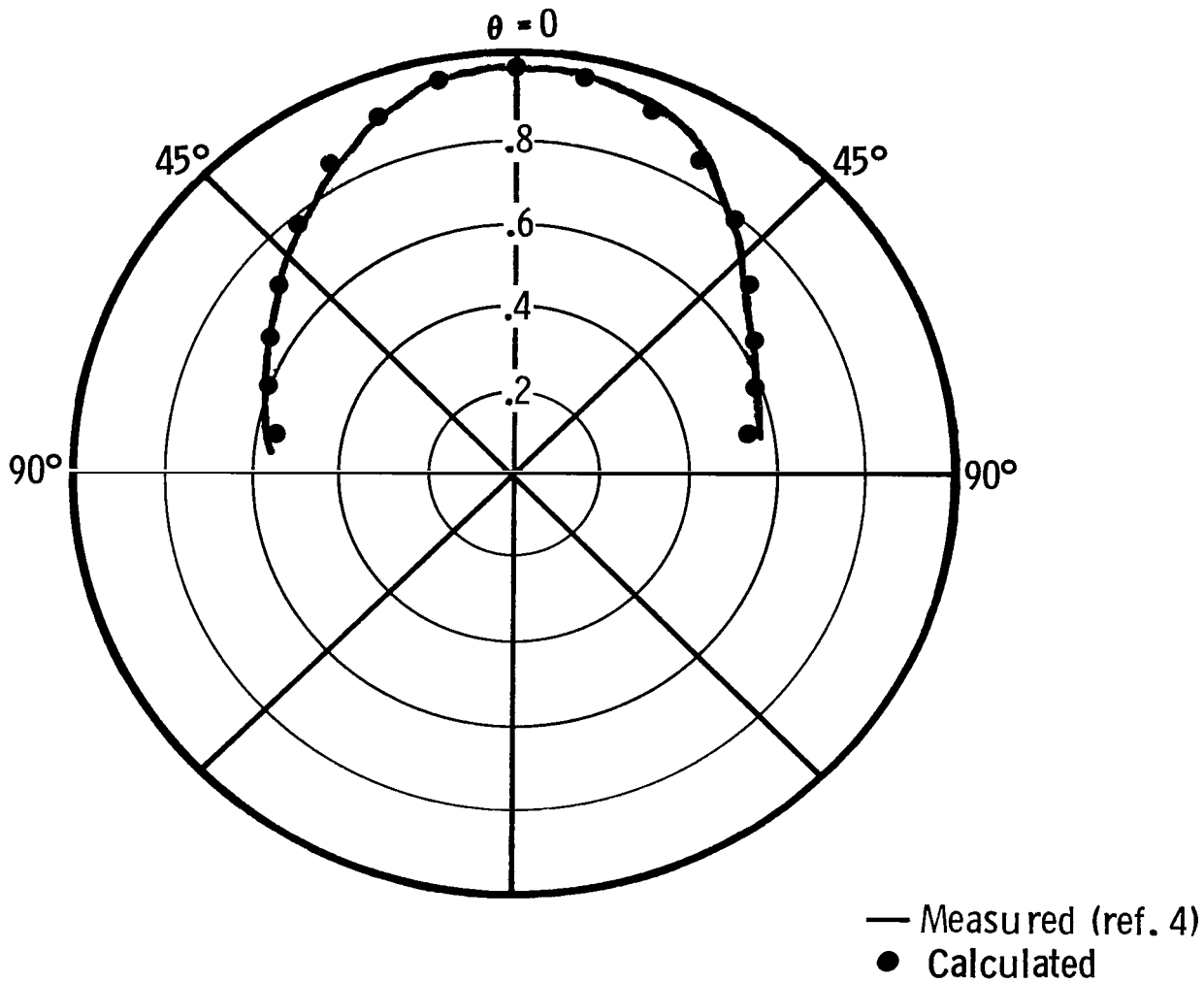

(b) E-plane pattern. $\phi = 0$.

Figure 25.- Concluded.

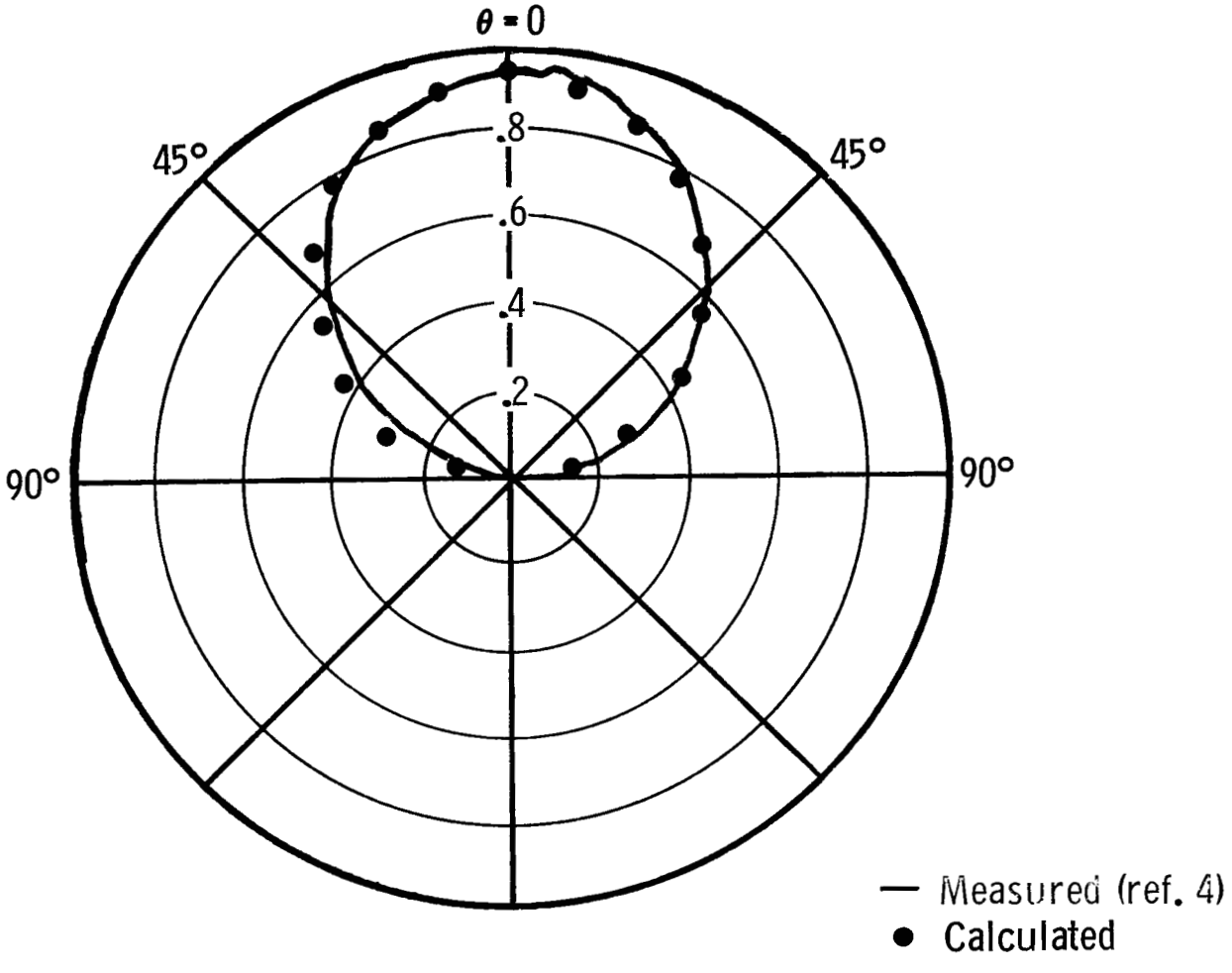

(a) H-plane pattern. $\phi = \pi/2$.

Figure 26.- Radiation pattern for 804-MHz rectangular-patch antenna. W_x = 11.43 cm; W_y = 7.6 cm; z' = d = 0.158 cm; ε_r = 2.62.

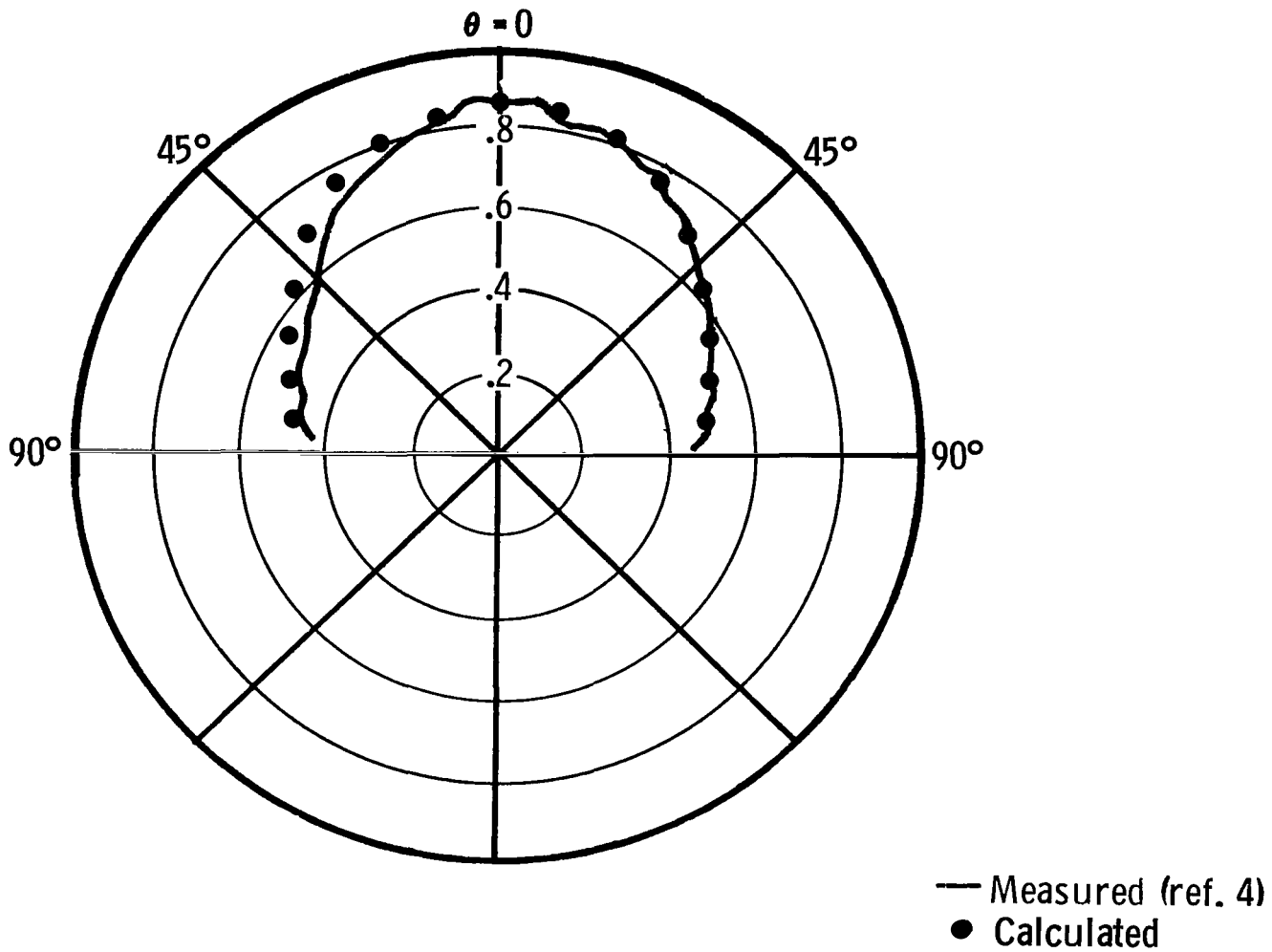

(b) E-plane pattern. $\phi = 0$.

Figure 26.- Concluded.

1. Report No.	2. Government Accession No.	3. Recipient's Catalog No.
NASA TP-2276		

4. Title and Subtitle	5. Report Date
ANALYSIS OF RECTANGULAR MICROSTRIP ANTENNAS	March 1984
	6. Performing Organization Code: 506-58-23-01
7. Author(s): M. C. Bailey and M. D. Deshpande	8. Performing Organization Report No.: L-15698
	10. Work Unit No.
9. Performing Organization Name and Address: NASA Langley Research Center, Hampton, VA 23665	11. Contract or Grant No.
	13. Type of Report and Period Covered: Technical Paper
12. Sponsoring Agency Name and Address: National Aeronautics and Space Administration, Washington, DC 20546	14. Sponsoring Agency Code

15. Supplementary Notes

M. C. Bailey: Langley Research Center, Hampton, Virginia.
M. D. Deshpande: The George Washington University, Joint Institute for Advancement of Flight Sciences, Hampton, Virginia.

16. Abstract

The problem of microstrip antennas covered by a dielectric substrate is formulated in terms of coupled integro-differential equations with the current distribution on the conducting patch as an unknown quantity. The Galerkin method is used to solve for the unknown patch current. Using the present formulation, the radiation pattern, the resonant frequency, and the bandwidth of a rectangular microstrip antenna are computed. Design data for a rectangular microstrip antenna are also presented.

17. Key Words (Suggested by Author(s))	18. Distribution Statement
Antennas Microstrip Electromagnetics Resonant frequency Radiation patterns Bandwidth	Unclassified - Unlimited Subject Category 32

19. Security Classif. (of this report)	20. Security Classif. (of this page)	21. No. of Pages	22. Price
Unclassified	Unclassified	58	A04

For sale by the National Technical Information Service, Springfield, Virginia 22161 NASA-Langley, 1984

5 1 1J,D, 840314 S00903DS
DEPT OF THE AIR FORCE
AF WEAPONS LABORATORY
ATTN: TECHNICAL LIBRARY (SUL)
KIRTLAND AFB NM 87117